

# **DLpN: Single-Shell NODDI Using Deep Learner Estimated Isotropic Volume Fraction**

*Abrar Faiyaz<sup>1</sup>, Marvin Doyley<sup>1,2,3</sup>, Giovanni Schifitto<sup>2,4</sup>, Jianhui Zhong<sup>2,3,5</sup>, Md Nasir Uddin<sup>4</sup>*

<sup>1</sup> Department of Electrical and Computer Engineering, University of Rochester, Rochester, NY, USA

<sup>2</sup> Department of Imaging Sciences, University of Rochester, Rochester, NY, USA

<sup>3</sup> Department of Biomedical Engineering, University of Rochester, Rochester, NY, USA

<sup>4</sup> Department of Neurology, University of Rochester, Rochester, NY, USA

<sup>5</sup> Department of Physics and Astronomy, University of Rochester, Rochester, NY, USA

## **Address Correspondence to:**

Md Nasir Uddin, PhD

Department of Neurology

University of Rochester

601 Elmwood Ave

Rochester, NY 14642

Phone: 585-275-5885

Email: [nasir\\_uddin@urmc.rochester.edu](mailto:nasir_uddin@urmc.rochester.edu)

## Highlights

- Proposed DictNet leverages prior fiso estimation.
- Subsequently DLpN enables reliable single-shell NODDI estimation with derived fiso.
- DLpN derived single-shell NODDI maps are comparable with multi-shell NODDI.
- DLpN may allow single-shell NODDI estimation for retrospective *in vivo* studies.

## Abstract

Neurite orientation dispersion and density imaging (NODDI) enables assessment of intracellular, extracellular and free water signals from multi-shell diffusion MRI data. It is an increasingly popular and insightful approach to characterize the brain tissue microstructure. Single-shell reconstruction for NODDI parameters has been discouraged in previous literature based on failure when fitting especially for the neurite density index (NDI). Here, we investigated the possibility to create robust NODDI parameter maps with single-shell data, using isotropic volume fraction (fiso) as prior. We made the prior estimation independent of NODDI model constraint using a dictionary based deep learning approach. First, we proposed a stochastic sparse dictionary-based network, DictNet in predicting fiso. In single-shell cases, fractional anisotropy (FA) and T2 signal without diffusion weighting ( $S_0$ ) were incorporated in the dictionary for fiso estimation. Then, NODDI framework was used in a prior setting to estimate the NDI and orientation dispersion index (ODI). Using both synthetic data simulation and human data collected on a 3T scanner, we compared the performance of our dictionary based deep learning prior NODDI (DLpN) with original NODDI method for both single-shell and multi-shell data. Our results suggest that DLpN derived NDI and ODI parameters for single-shell protocols are comparable with original multi-shell NODDI, and protocol with  $b=2000$  s/mm<sup>2</sup> (P2) performs the best (error ~2% in white matter

and ~4% in grey matter). This may allow NODDI evaluation of retrospective studies on single-shell data by additional scanning of two subjects for DictNet  $f_{ISO}$  training.

## Keywords

Single-shell NODDI; Diffusion MRI; Neurite Density; Orientation Dispersion; Sparse Dictionary Learning; Deep Learning.

## Abbreviations

dMRI, diffusion MRI; DTI, diffusion tensor imaging; FA, fractional anisotropy; AD, axial diffusivity; RD, radial diffusivity; MD, mean diffusivity; NODDI, neurite orientation dispersion and density imaging; CSF, cerebrospinal fluid; NDI, neurite density index; ODI, orientation dispersion index;  $f_{ISO}$ , isotropic volume fraction; AMICO, Accelerated Microstructure Imaging via Convex Optimization; MLP, multiple layer perceptron; LTSM, long short-term memory; IHT, iterative hard thresholding; IQT, information quality transfer; T2w, T2-weighted; DLpN, Deep Learning prior NODDI; DictNet, dictionary based deep network; GM, grey matter; WM, white matter.

## 1. Introduction

Neurites are the structural units of the brain, comprising of axons and dendrites. Alterations in neurite structure occur during brain development, normal aging, and in several neurodegenerative disorders (Conel, 1947; Dutta and Trapp, 2007; Fiala et al., 2002; Jacobs et al., 1997). Histological analysis of postmortem brain tissue is regarded as the most reliable means to quantify the neurite morphology and understand such alterations in neurological diseases. Some limitations of the histological assessment include variability in tissue sampling and longitudinal access to tissue. Furthermore, the tissue preparation may cause changes in the morphology. In living individuals there are obvious ethical limitations in tissue procurement. Conversely, MRI is an excellent modality to provide information about neurites *in vivo* non-invasively with whole brain coverage, and faster image acquisition compared to the analysis of histological sections (Alexander et al., 2019).

Diffusion MRI (dMRI) can provide quantitative measures of tissue microstructure by probing molecular water diffusion in the brain (Beaulieu, 2002). Diffusion tensor imaging (DTI) (Basser et al., 1994), a widely used dMRI technique, is based on a gaussian water displacement distribution. DTI metrics such as fractional anisotropy (FA) and diffusivities (axial diffusivity AD, radial diffusivity RD, and mean diffusivity MD) are sensitive to alterations of tissue properties such as cellular density, axon diameter, myelin and water content (Beaulieu, 2002). However, these metrics are not specific to any particular tissue properties since the DTI model does not account for restricted and hindered water diffusion (Assaf and Pasternak, 2008; Pasternak et al., 2018).

To address these limitations, advanced multi-shell dMRI technique (i.e., diffusion weighted, DW images acquired with multiple b-values) such as the neurite orientation dispersion and density

imaging (NODDI) was developed (Zhang et al., 2012). NODDI, a non-Gaussian model, assumes three types of tissue compartments: intra-neurite, extra-neurite, and cerebrospinal fluid (CSF) that enables the estimation of the neurite density index (NDI), orientation dispersion index (ODI) and isotropic volume fraction (fiso). The NDI measures the neurite density in both axons and dendrites while ODI measures the variability of neurite orientation. These two key indices have been histologically validated by correlating NDI with optical myelin staining and ODI with Golgi staining analysis (Jespersen et al., 2010; Jespersen et al., 2012). Several previous studies have demonstrated that NODDI outperforms DTI and provides more insight into the disease processes, normal neurodevelopment and aging (Grussu et al., 2015; Timmers et al., 2016).

However, non-linear NODDI model fitting is computationally intensive and may need parallel computing clusters and long computational time for DW data with good resolution (typically  $\sim$ 65 hours) (Daducci et al., 2015). To reduce the computation time, the problem has been reformatted in a dictionary-based framework by Daducci (Daducci et al., 2015) with Accelerated Microstructure Imaging via Convex Optimization (AMICO). The linearization of the non-linear NODDI problem via AMICO made the fitting faster by four orders of magnitude and the calculated microstructural parameters were demonstrated to preserve accuracy and precision with high correlation ( $r^2 > 0.81$ ). This also allowed for the sparse reconstruction strategies to be utilized with deep learning approaches to solve the NODDI problem. However, this sparse representation of the diffusion signal in AMICO still requires a large number of diffusion gradients with multi-shell protocol similar to NODDI in order to estimate the microstructural parameters.

Compared to DTI, the NODDI model requires a larger number of gradient directions (e.g.,  $\geq 90$  directions) with multi-shell protocols of at least two b-values (e.g.,  $b=1000$  and  $2000$   $\text{s/mm}^2$ ) (Zhang et al., 2012). In order to make the protocol clinically feasible, efforts have been made to

reduce the number of diffusion gradients using deep learning (Golkov et al., 2016; Ye, 2017; Ye et al., 2019). Additionally, compared to conventional methods, the other major advantages of deep learning approaches include that the reconstruction of NODDI parameter maps can be very fast once the training is completed, and noise can be reduced via spatial consistency of the DW signals. Golkov *et al.* used a multiple layer perceptron (MLP) with three hidden layers to estimate NODDI microstructures from data with multi-shell protocols (Golkov et al., 2016). Subsequently, Ye (Ye, 2017) proposed an optimization-based deep learner (Domke, 2012) which uses the *iterative hard thresholding* (IHT) (Blumensath and Davies, 2008) in order to calculate the sparse representation using learned weight vectors. The network was further improved for the estimation accuracy by incorporating historical information in an adaptive process for the update of sparse codes that modified the *long short-term memory* (LSTM) units with IHT process (Ye et al., 2019). However, multi-shell data has been used for both training and test cases for these methods because existing literature highlights that single-shell NDI, ODI and fiso fitting is ill-posed with NODDI.

Recently, Alexander et al. (Alexander et al., 2017) proposed a computational imaging technique called information quality transfer (IQT), which first showed the potential of microstructure reconstruction using DTI tensors calculated from standard single-shell data. They built parametric regression trees based on the calculated diffusion tensor features manually to train distributed leaf weight vectors on NODDI generated outputs. In short, the method divided the hyperparameter space based on spatial DTI features and learned discrete weight vectors at the leaf nodes to map microparameters. However, this was a DTI feature-based end to end black box learning and no ground validation was provided for single-shell reconstruction. Nonetheless, the work suggests that DTI features have the potential to estimate NODDI microparameters with single-shell data. Another study by Edwards et al. (Edwards et al., 2017) derived NODDI-DTI

relationship once  $f_{iso}$  was set to a fixed zero using single-shell data in regions with less to no free water contamination. These findings reinforced our hypothesis that prior  $f_{iso}$  may be useful in reconstructing NDI and ODI with single-shell data.

We hypothesized that with an estimation of  $f_{iso}$ , it might be possible to obtain well-posed NDI and ODI maps with single-shell DW data. For  $f_{iso}$  estimation, we were motivated to incorporate DTI scalar and T2-weighted (T2w) signal in our dictionary from previous work on IQT (Alexander et al., 2017). To the best of our knowledge, no prior study has validated single-shell NDI and ODI reconstruction with the originally proposed NODDI model which formulates the objective function with a maximum Rician log likelihood framework. The purpose of this work is to investigate NODDI dependency on multi-shell data and to understand if the stochastic sparse dictionary based deep learning approach could estimate the fundamental parameter sensitive to multi-shell data in simulation and *in-vivo*. Using both synthetic and *in vivo* data, we formulate a sparse dictionary for  $f_{iso}$ , with a learner that replaces the iterations of the Iterative Hard Thresholding (IHT) for sparse dictionary learning with a stochastic layer. Corresponding DTI scalar FA and T2w signal  $S_0$  were utilized in building the dictionary for single-shell  $f_{iso}$  estimation. We then compare the performance of single-shell protocol reconstructions with multi-shell ones generated with dictionary based Deep Learning prior NODDI (DLpN) and NODDI for NDI and ODI.

## 2. Materials and Methods

In this section, we first briefly review the background of NODDI tissue model. Then we describe our deep learning prior NODDI fitting. Finally, we present the training and validation strategies using in synthetic simulation and *in vivo* data. HCP data source and details have been elaborated in Section 2.4.

### 2.1 NODDI tissue model

DTI fitting assigns one apparent diffusion coefficient (ADC) for a single voxel where NODDI tissue model hypothesizes three different microenvironments, where the ADC in each hypothesized compartment is different. So, for an MR signal for a given voxel, the associated microenvironments are extracellular, intracellular and free-standing water in different configurations. The related diffusion coefficients for three compartments are respectively  $d_{\parallel}$ ,  $d_{\perp}$  and  $d_{ISO}$ . The underlying assumption is  $d_{\parallel}$  and  $d_{ISO}$  can be assumed with the properties known from in-vivo cases (Zhang et al., 2012). Therefore, the NODDI tissue model is stated as follows –

$$A = (1 - f_{ISO})\{NDI \cdot A_{IC} + (1 - NDI) \cdot A_{EC}\} + f_{ISO}A_{ISO} \quad (1)$$

where, for intracellular (IC) compartment,

$$A_{IC} = \int_{S^2} f(\vec{n}) e^{-b d_{\parallel} (q \cdot n)^2} d\vec{n} \quad (2)$$

where  $b$  = b-value,  $q$  = b-vector,  $n$  = samples of directions on a sphere on which the integration is done. Probability of finding orientation directed along  $n$  when  $\mu$  and  $\kappa$  known,

$$f(\vec{n} \mid \vec{\mu}, \kappa) = M \left( \frac{1}{2}, \frac{3}{2}, \kappa \right)^{-1} e^{\kappa(\vec{\mu} \cdot \vec{n})^2} \quad (3)$$

In the Eq. 3,  $M$  is defined as a confluent hypergeometric function.

For the extracellular (EC) compartment,

$$A_{\text{EC}} = e^{-\mathbf{b}\mathbf{q}^T D_{\text{EC}}(f, \text{NDI}) \mathbf{q}} \quad (4)$$

where,

$$D_{\text{EC}}(f, \text{NDI}) = \int f(\vec{n}) D_h(\vec{n}, \text{NDI}) d\vec{n} \quad (5)$$

Equation 4 was solved with its analytic form elaborated in (Zhang et al., 2012).

For the isotropic compartment,

(6)

$$A_{\text{ISO}} = e^{-b \cdot d_{\text{ISO}}} \text{ where } d_{\text{ISO}} = 3.0 \times 10^{-3} \text{ mm}^2 \text{ s}^{-1}$$

ODI is dependent on  $\kappa$ , known as the concentration parameter associated with the Watson distribution defined in (3) and calculated as follows-

$$\text{ODI} = \frac{2}{\pi} \arctan\left(\frac{1}{\kappa}\right) \quad (7)$$

The signal model with multi-shell protocol uses ground-truth parameters to synthesize the diffusion weighted signal and is further synthesized with Rician noise with regulated signal to noise ratio (SNR). NODDI relies on maximum Rician log-likelihood framework to fit the measured diffusion signal obtained with the NODDI multi-shell protocol to reconstruct NDI, ODI and  $f_{\text{ISO}}$ .

## 2.2. Deep Learning prior NODDI (DLpN)

The proposed DLpN is a deep learner based approach that conditions NODDI mapping with single-shell dMRI data where  $f_{\text{ISO}}$  is obtained as a prior from the learner. Prior estimation is performed using DictNet (Section 2.3) network, as shown in Figure 1. In the NODDI model, the diffusion signal synthesized with NDI and ODI parameters are weighted with  $1-f_{\text{ISO}}$  in the framework (Zhang et al., 2012) . Thus, if  $f_{\text{ISO}}$  estimation is made independent and fixed, NODDI becomes stable and unique in terms of single-shell diffusion data. The proposed approach separates

the estimation of  $f_{\text{ISO}}$  adopting a dictionary based deep learning strategy termed as “DictNet”, and then fits for the other non-linear parameters posed in the NODDI problem with the Rician loglikelihood framework (Zhang et al., 2012). In this framework, the NODDI toolbox (Zhang et al., 2012) has been modified to fit the requirement. Once we have an approximation of the  $f_{\text{ISO}}$ , the Rician loglikelihood framework can be employed to solve the inverse problem of identifying NDI and ODI of the respective tissue compartment. With respect to the estimated likelihood based on the DW signal, the initial parameters need to be updated, which initialized as zero for the first iteration. NODDI toolbox makes use of grid search approach, which generates a possible set of parameters and selects the initial set of parameters based on the maximum calculated likelihood. Gradient descent then regulates the search path on the hyperparameter space. Since  $f_{\text{ISO}}$  is already approximated from the deep learning framework, the grid search complexity is reduced per voxel.

We fit the parameters by maximizing the Rician loglikelihood framework as follows:

$$L(\text{NDI}, \kappa, \theta, \phi \mid f_{\text{ISO}}, d_{\parallel}, d_{\text{ISO}}) = -\log \prod_{i=1}^N \frac{M_i}{\sigma^2} e^{-\frac{(M_i^2 + A^2)}{2\sigma^2} I_0\left(\frac{AM_i}{\sigma^2}\right)} \quad (8)$$

which is similar to the NODDI problem, except that the initial prior is estimated with DictNet.

In the Eq. (8),  $A$  is synthesized and  $M$  is the measured signal. NDI is the neurite density index,  $\kappa$  term is inversely proportional to ODI (Eq. 7),  $f_{\text{ISO}}$  is the isotropic volume fraction, and  $\sigma$  is the estimated standard deviation from the measured signal per voxel.

### 2.3 DictNet

DictNet is a sparse dictionary based learning strategy that has been devised based on previous works (Ye, 2017; Ye et al., 2019) to approximate  $f_{\text{ISO}}$ . Typically, with a known sparse dictionary  $\Phi$ , the coefficients  $f$  can be assessed by an  $\ell_1$ -norm regularized least squares problem

$$\hat{f} = \arg \min_{f \geq 0} \| \Phi f - y \|_2^2 + \lambda' \| f \|_0 \quad (9)$$

where,  $\lambda'$  is an adjustable parameter to control the sparsity level of  $f$ . We can resolve this using Iterative Hard Thresholding (IHT) algorithm (Blumensath and Davies, 2008) as follows-

$$f^{t+1} = H_\lambda(Ld_{\text{in}} + Df^t) \quad (10)$$

where,  $t$  is the iterative index,  $L$  and  $D$  are layers determined by the sparse dictionary  $\Phi$ , and  $H_\lambda(\cdot)$  is a thresholding function. The threshold is defined by a parameter  $\lambda$  which is related to  $\lambda'$ ,  $d_{\text{in}}$  is the normalized diffusion signal cascaded with  $3 \times 3 \times 3$  spatial data. Previously proposed deep architecture models, Microstructure Estimation using a Deep Network (MEDN), advanced MEDN (PMEDN) (Ye, 2017) and MESC-nets (Ye et al., 2019) used 8 iterations of IHT in its original and modified form, respectively.

However, this iterative process can be redundant. By replacing the iterative scheme with a constant stochastic layer, we can eliminate unnecessary weight vectors thereby saving memory and training time as follows for the estimation of  $f_{\text{ISO}}$  of a voxel without hindering the performance.

$$f = H_\lambda(Ld_{\text{in}} + Dd) \quad (11)$$

This is illustrated in Eq. (11), where  $d$  is the constant stochastic vector, the basis on which the dictionary is built; and  $L$  and  $D$  are the same matrices determined by dictionary  $\Phi$ . Then, the generated coefficient vector  $f$  contributes to a fully connected feedforward network to estimate the specified microparameter i.e.,  $f_{\text{ISO}}$ . For single shell fitting  $f$  contributes with additional FA and, T2w or  $S_0$  layers and contribute in the final estimation with a thresholded relu function. Microstructure estimation deep learners like MESCnet (Ye et al., 2019) needs 47GB RAM whereas proposed DictNet takes less than 4GB RAM and  $\sim 30$  minutes training time. In comparison

with PMEDN it is also 8 times less bulky, as the stochastic vector layers are sufficient to generate the specified parameters. Figure 2 illustrates the error per epoch in single and multi-shell cases and compares DictNet with PMEDN in training and validation.

#### ***2.4. Subjects and MR acquisition***

##### ***2.4.1 In vivo Data***

De-identified MRI images from 8 randomly selected subjects from the publicly available Human Connectome Project (HCP) dataset provided by WU-Minn HCP, release-Q3 (Van Essen et al., 2013) were used for this study. Written informed consent was collected from all subjects and the study was approved by the institutional review board ([https://db.humanconnectome.org/data/projects/HCP\\_1200](https://db.humanconnectome.org/data/projects/HCP_1200)). Multi-shell dMRI images were acquired using a 3T MRI scanner (Connectome, Siemens, Erlangen, Germany) using spin-echo echo planar imaging (SE-EPI) sequence (TR=5520 ms, TE=89.5 ms, field of view=210 ×180, voxel size = 1.25×1.25×1.25 mm<sup>3</sup>, multiband factor = 3, bandwidth=14887 Hz/pixel, 90 gradient directions for each shell: b-values =1000, 2000, and 3000 s/mm<sup>2</sup>, and 18 non-diffusion weighted images with b=0 s/mm<sup>2</sup>, and scan time for each shell was around 9:50 min. Subject data were corrected for bulk motion, susceptibility-induced and eddy current distortions (Glasser et al., 2013). Further details of scan parameters and study protocols can be found in <http://protocols.humanconnectome.org/>.

All the protocols used in this work are tabulated in Table 1. In this work, microstructure parameters (NDI, ODI, fiso) computed by NODDI (Zhang et al., 2012) with Pall (i.e., full set of 270 diffusion gradients) were considered as pseudo ground-truth.

##### ***2.4.2 Synthetic Data***

In order to evaluate the DLpN framework together with NODDI we utilized known ground-truth tissue microstructures for different protocols and synthesized MR signals, as similar to the approach in the original NODDI paper (Zhang et al., 2011), with  $f_{ISO}=0$  as well as *with* additional  $f_{ISO}$  cases reported in Table 2. The  $f_{ISO}$  is negligible in WM (Veraart et al., 2019), but in order to see the underlying effect of GM structures and free water contaminated ROIs, additional  $f_{ISO}$  cases of 0.12, 0.4, 0.75, 1 were added in the simulation experiment. The simulation strategy is described in (Zhang et al., 2012); We have used the publicly available NODDI toolbox (version 1.01, [https://www.nitrc.org/projects/noddi\\_toolbox](https://www.nitrc.org/projects/noddi_toolbox)) and modified the initialization to fit the simulation needs for different diameters,  $a$ , and set  $f_{ISO}$  as prior when fitting for a voxel. To simulate WM and GM tissue configurations, model parameters were set to representative values for both tissue types. The selected set of parameters in simulation is also reported in Table 2. The parameter set accounts for 400 different microstructural configurations in 254 uniformly sampled q-space directions termed as mean orientation,  $\mu$ . Different mean orientations were used to create synthetic training and test dataset. FSL’s “dtifit” tool was used to calculate the FA and raw T2 signal without diffusion weighting ( $S_0$ ) of the synthesized signals.

### **2.5. DictNet: Train, Validation and Test**

Among 8 randomly selected subjects, we used HCP dMRI data from 2 subjects as training set, and the remaining subjects were used for testing. The number of training subjects was chosen based on results reported in Supplementary Figure S1. Here we showed that if the number of training subjects is greater than three, the network is more prone to overfitting. Accordingly, based on these results two subjects were selected for training. The training was voxel-wise with NDI, ODI and  $f_{ISO}$  with different number of training subjects and error was reported on four test subjects. Since

the training is performed voxel-wise, we had masked brain voxels of 2 subjects (each of  $145 \times 174 \times 145$ ) for training where 15% of the data was used for cross-validation for each epoch, with maximum of 10 epochs. In the train/test phase, the DW signal was normalized with mean non-diffusion weighted b0 image and used as input for the network.

In Figure 2, fiso loss is demonstrated in training and validation of (a) Single and (b) Multi-shell cases in DictNet and extended Microstructure Estimation Deep network, PMEDN (Ye, 2017). Stochastic initialization and training improvise objective learning for DictNet. Training and validation errors show similar performance in training for DictNet and PMEDN. The memory required for DictNet was 8 folds less and faster, compared with PMEDN.

The pseudo ground-truth microstructure parameters (NDI, ODI, fiso) were computed by NODDI (Zhang et al., 2012) using the full set of 270 diffusion gradients. DictNet is capable of training and estimating all the 3 microparameters. However, for DLpN reconstruction, since we focus on retrieving fiso prior, thus only the fiso prior is trained and estimated from the DictNet. The other pseudo ground truth parameters- NDI and ODI were used to evaluate DLpN reconstructions. Initial training for DictNet was done on pseudo ground-truth fiso data. This dictionary trained with HCP data was further trained with the ground truth simulated DW data for 5 epochs in order to sensitize it for the synthetic training dataset. In order to make the dictionary well-posed for single-shell cases, FA was obtained for both synthetic data and *in vivo* using a single-shell protocol and, FA and S<sub>0</sub> were used in building fiso dictionary.

### 3. Results:

#### 3.1 Synthetic data simulation

We reconstructed the NODDI microparameters from synthesized DW signals with protocols defined in Table 1 by initializing the model with known fiso with random  $\pm 5\%$  deviation. The

simulation results obtained with  $f_{iso}=0$  were the same as in the original NODDI paper (Zhang et al., 2012) (not shown). However, with additional  $f_{iso}$  cases we found different result and our precursory investigation with synthetic data simulation supports that NDI and ODI microparameters can be reconstructed reliably from single-shell DW imaging data if  $f_{iso}$  is used as prior. The NODDI microparameter estimation results with  $f_{iso}=0$  and additional  $f_{iso}$  cases are described below.

### ***3.1.1 NDI and ODI estimation with and without $f_{iso}$ prior***

Figure 3 illustrates the NDI reconstruction for different protocols with DLpN and original NODDI fitting. However, using the synthetic data generated with additional  $f_{iso}$  plausible cases, we revealed that NODDI fitting resulted in NDI deviation (upward bias) from the ground-truth with multi-shell protocols for NDI ground-truths of  $\leq 0.4$  (Figure 3). We also found the downward bias with high variance for single-shell protocols reconstructed with NODDI model except at the ground-truth NDI=0.2.

In contrast, we observed that  $f_{iso}$  prior reconstruction in DLpN can result in NDIs with markedly improved accuracy and precision in both single- and multi-shell cases. This illustrates that independent estimation of  $f_{iso}$  may lead to a better estimation of NDI. However, some deviations from the ground-truth values were observed in the case of protocol P2 and P3 at lower NDI. This could be because measurements at high b-values may not support tortuosity constraints (in the GM or lower NDI region) posed by the NODDI model (Novikov et al., 2018).

Figure 4 illustrates that ODI reconstruction with proposed DLpN and NODDI fitting for different protocols and ground-truth values. We found similar trends in ODI for both DLpN and NODDI fitting, however DLpN had a lower variance for all protocols. Consistent with NODDI paper (Zhang et al., 2012), biasness and variance are low for the ground truth of  $< 0.5$ . Variability

of ODI for higher ground-truth values are related to the ODI itself. The orientation distributions corresponding to very large ODIs are not very different from one another and the high variance reflects the lack of difference. It should be noted higher ODI corresponds to highly dispersed neurites mainly residing in GM and previously shown to improve with number of gradients used without any dependency on the number of shells (Zhang et al., 2012).

### **3.1.2 DictNet and NODDI $f_{iso}$ estimation**

We validated the estimation of  $f_{iso}$  with DictNet at all defined ground-truth values in Table 2. We found a reasonable estimation of  $f_{iso}$  with DictNet and the fitting was well-posed for the multi-shell cases with protocol P12 and Pall and, single-shell cases P1 and P2 where FA and  $S_0$  contributed in the dictionary building of DictNet, presented in Figure 5. However, the estimated  $f_{iso}$  values with single-shell DictNet cases without FA and  $S_0$  contribution were found ill-posed (not shown). We further reconstructed the same simulated dataset with NODDI and found that, both single- and multi-shell  $f_{iso}$  estimation was ill-posed due to the NODDI model constrain for several cases shown in the same Figure 5. For multi-shell case, the fitting was ill-posed for some cases in  $NDI < 0.6$ . This indicates  $f_{iso}$  estimation to be constrained by the NODDI model and pose restriction in accurate parameter estimation probably due to initialization bias or local minima problem in non-linear fitting. However, Figure 5 simulation suggests that it is safe to estimate  $f_{iso}$  independently in a prior setting using DictNet with protocols P1, P2, P12 and Pall.

## **3.2 Human brain data**

Figure 6A represents  $f_{iso}$  maps reconstructed using DictNet and NODDI for single- and multi-shell protocols. The  $f_{iso}$  difference maps between the pseudo ground-truth (i.e., NODDI<sub>Pall</sub>) and DictNet along with NODDI with both single- and multi-shell reconstructions are shown in Figure

6B. From the difference maps, it is evident that DictNet outperforms NODDI for single-shell protocols (P1, P2, P3) as well as for two-shell protocols (P12, P13, P23) with respect to the pseudo ground-truth. Similarly, The NDI and ODI maps were shown for DLpN and NODDI fittings with different protocols in the human brain respectively in Figure 7A and Figure 8A; and corresponding difference maps are shown in Figures 7B and 8B.

Comparison of DictNet derived  $f_{iso}$  and DLpN derived NDI and ODI values for several GM and WM ROIs obtained with single-shell DLpN (P1, P2, P3) and NODDI<sub>Pall</sub> protocols are provided in the supplementary Figures S2, S3 and S4. Pearson correlations of the data combined across all test subjects for WM and GM ROIs between NODDI<sub>Pall</sub> and DLpN based NDI and ODI and DictNet derived  $f_{iso}$  for both single- and multi-shell protocols revealed strong and highly significant correlations (Supplementary Figure S5). DLpN based NDI maps for single-shell protocols indicated strong correlations with NODDI<sub>Pall</sub>: DLpN<sub>P1</sub> ( $r^2=0.875$ ), DLpN<sub>P2</sub> ( $r^2=0.927$ ), DLpN<sub>P3</sub> ( $r^2=0.944$ ), suggesting higher b-values in single-shell can reconstruct close to NODDI<sub>Pall</sub>. The DLpN based ODI maps showed very strong correlations with NODDI<sub>Pall</sub> ( $r^2>0.93$ ) and found to be similar to those reported in (Zhang et al., 2012) for both single and multi-shell cases.

The performance of single-shell  $f_{iso}$  with DictNet, and NDI and ODI with DLpN have been further assessed for both WM and GM by means of the percentage error (mean and standard deviation) as presented in Figure 9. The percentage errors were calculated for each microparameter from each protocol with respect to the pseudo ground-truth NODDI<sub>Pall</sub> protocol and reported for the mean for the ROIs. The single-shell protocols had less than 5% error with low variance in estimating NDI and more or less 10% for ODI (Figure 9B,C).

As part of an exploratory investigation, we noticed that multi-shell NDI reconstruction with both NODDI and DLpN are noisy and we assume this might lead to overestimation of the

parameter, highlighted in Supplementary Figure S6. White arrows indicate overestimated NDI regions in NODDI<sub>Pall</sub> that seems to be recovered with single-shell fitting DLpN<sub>P2</sub> (Supplementary Figure S6). In addition, Supplementary Figure S7 reports NODDI<sub>Pall</sub> shown to estimate  $f_{iso} = 0$  (highlighted in blue) near GM ROIs. This leads to the possibility that  $f_{iso}$  estimation in these regions is biased with model constraint for NODDI, highlighted in the simulation result (Section-3.1.2). As there is a high chance of free water or CSF contamination near the GM regions, so expected  $f_{iso}$  in these regions are close to 0 but should not be exactly 0. NODDI nonlinear parametric search seems to have lowered  $f_{iso}$  estimation by accounting for higher dispersion in these regions.

## 4. Discussion

In this work, we demonstrated that NODDI non-linear fitting is capable of reconstructing NDI and ODI using single-shell protocols with the use of prior  $f_{iso}$  both in simulation and *in vivo* experiments. In order to generate  $f_{iso}$ , we devised a network, motivated by the IHT strategy used in recent studies (Ye, 2017; Ye et al., 2019). We proposed a non-iterative scheme of IHT where a constant stochastic layer determines the learning of dictionary coefficients along with spatial-angular sparse vector generated from the initial input layer. Then, the generated coefficient vector contributes to a fully connected feed-forward network to estimate the  $f_{iso}$ . To account for single-shell fitting, additional layers with DTI metric FA and, T2w or S<sub>0</sub> signal contribution was added in building the dictionary. The overall procedure drastically reduces memory requirements and training time compared to the previous approaches (Ye, 2017; Ye et al., 2019), and preserves the estimation accuracy and precision in estimating  $f_{iso}$  compared to the ground-truth data.

Using both simulation and *in vivo* data experiments, we evaluated the feasibility of our proposed DLpN approach for single-shell NODDI parameters mapping, and compared the results with the original multi-shell NODDI<sub>Pall</sub> fitting. The results from both experiments indicated that single-shell NDI and ODI reconstructions are possible with good accuracy. Our simulation results revealed that DictNet generated single- and multi-shell fiso values were well-posed whereas on the same dataset NODDI showed ill-posed behavior in fiso estimation likely due to NODDI model constraint. DLpN based NDI and ODI reconstructions for single-shell protocols were very close to the ground-truth values and consistently outperformed the original NODDI fittings.

Using the *in vivo* data, we found that DLpN based NDI values in WM were underestimated by 0 to 5% using the single-shell protocols relative to the pseudo ground-truth NODDI<sub>Pall</sub>. On the other hand, GM showed ~2% overestimation for DLpN<sub>P1</sub> and less than 1% error for DLpN<sub>P2</sub> while ~7% underestimation for protocol DLpN<sub>P3</sub> compared to NODDI<sub>Pall</sub>. For ODI, DLpN<sub>P2</sub> showed the lowest error (~2% in WM and by ~4% in GM) while DLpN<sub>P1</sub> and DLpN<sub>P3</sub> showed higher bias (underestimated by 10-13% in DLpN<sub>P1</sub>, while overestimated by ~11% for DLpN<sub>P3</sub> in WM and by ~3.5% in GM). Interestingly, DLpN<sub>P2</sub> had a minimum error for both NDI and ODI (less than 4%), even when it showed to have a percentage-wise higher error in fiso estimation (~25%) with strong correlations ( $r^2 > 0.9$ ) compared to the pseudo ground-truth NODDI<sub>Pall</sub> (Figure 9 and Supplementary Figure S5). It seems DictNet<sub>P2</sub> identified a different set of fiso based on the built dictionary which retained the similar solution for NDI and ODI with DLpN<sub>P2</sub> as for NODDI<sub>Pall</sub>. DLpN<sub>P2</sub> has also removed the multi-shell fitting noise in the process. We also notice that NODDI<sub>Pall</sub> has shown to estimate higher fiso in WM ROIs than DictNet (P1, P2 and P3 cases) shown in Supplementary Figure S2. In addition, DLpN<sub>P2</sub> results in NDI and ODI closest to the pseudo ground-truth. and DictNet P2 has shown to estimate fiso among single-shell protocols that

resembles comparison with recently reported comparison of NODDI derived fiso and FWI derived FW values (Chad, 2019). So, in order to recreate NODDI<sub>Pall</sub> NDI and ODI maps, DLpN<sub>P2</sub> is recommended.

However, the possible explanations of some biases in single-shell P1 and P3 cases may attribute to several factors: first of all, DLpN<sub>P1</sub> NDI and ODI reconstruction was performed without accounting for gradient non-linearity which may have an effect for lower b-valued protocol, P1. Secondly, DictNet P3 fiso estimation was not as well-posed in simulation, probably due to the fact that higher b-value images are relatively noisier. Based on our simulation results DictNet P2 derived fiso (shown to be well-posed in simulation) performed best for our *in vivo* experiment in terms of generating NODDI<sub>Pall</sub> NDI and ODI maps.

There are some advantages of the DLpN approach. First, NDI and ODI maps become subject to improvement with DLpN if independent fiso or free water can be better estimated in future research with single or multi-shell cases. Second, the use of the single-shell protocol would reduce the scan time by more than 50% compared to standard NODDI acquisition. Thus, this approach might be useful to get NDI and ODI reconstructions using a clinical scanner and in a clinically feasible acquisition time for cases such as stroke, pediatric or emergency subjects with sufficient resolution. Third, the DLpN approach may be applied retrospectively on the existing data collected with a reasonable number of diffusion directions and appropriate b-value (say  $b=1000$  s/mm<sup>2</sup>), however prerequisites for using the existing dataset is that two new scans are required with the same scan parameters with two-shell protocol ( $b=1000, 2000$  s/mm<sup>2</sup>) to train for fiso. Nonetheless, in cases where additional scans are not possible, single-shell free water imaging (FWI) could be a potential source to generate fiso maps to do further analysis. However, we are aware that fiso estimated with single-shell FWI might be weakly posed, so another possible mitigation would be

using the Freewater EstimatoR using iNtErpolated iniTialization (FERNET) technique for fiso prior estimation using a regular protocol (Parker et al., 2020). Then DLpN<sub>P2</sub> can be used to recover NDI and ODI comparable with NODDI<sub>Pall</sub>.

The limitation of this study lies primarily on how accurately fiso training might be possible to generate a better dictionary. One mitigation could be generating ground-truth training data with phantoms that can be used to study FW per voxel as reported in a recent work (Farrher et al., 2020). This may help to account for scanner variables in fiso training which wasn't possible in simulation. Any further improvement in fiso estimation will directly improve NDI and ODI map with the DLpN approach using a single-shell or multi-shell protocol. Secondly, the DLpN processing time for either single-shell cases is currently 10 to 13 hours whereas the original NODDI model required 20 to 30 hours to process on our multicore setup (24 cores used for fitting). However, AMICO setup with our single-shell DLpN approach should be able to reduce the NDI and ODI processing time down to <30 minutes. The DLpN could further extend the current work via accurate quantification of fiso either using single-shell (preferably  $b=1000$  s/mm<sup>2</sup>) or multi-shell DW data ( $b<1500$  s/mm<sup>2</sup>) in clinically feasible MRI scans. Future work will be needed for further single-shell NODDI advancement by mitigating some limitations by using T2 mapping as a prior for accurate NDI and fiso estimation, and reducing the number of diffusion gradients, as well as with advanced machine learning approaches that account for ill-posed problems.

## 5. Conclusions

We have proposed a dictionary based deep learning prior NODDI, DLpN for estimating NODDI parameter maps from single-shell dMRI data. This study segregates the parameter that relies on multi-shell and shows single-shell NDI and ODI is stable with fiso as prior. The resulting NODDI parameter maps are comparable with those reconstructed with the original multi-shell NODDI

model. Since fiso prior estimation is shown to be independent and well-posed when deep learning dictionary is constructed using corresponding FA and  $S_0$ , this approach may allow retrospective studies on existing single-shell dMRI data to evaluate NDI and ODI with the prerequisite of two additional scans for training DictNet.

## Acknowledgements

This work was supported by the National Institutes of Health (Grant Numbers: R01 AG054328, and R01MH118020). We would like to thank Alan Finkelstein for his careful linguistic scrutinization, editing and proofreading.

## Declaration of Competing Interest

The authors declare no competing interests.

## Author Contributions

**Abrar Faiyaz:** Conceptualization, Methodology, Software, Formal analysis, Writing - original draft, Writing - review & editing, Validation; **Marvin Doyley:** Resources, Writing - Review & Editing; **Giovanni Schifitto:** Resources, Writing - Review & Editing; Funding acquisition; **Jianhui Zhong:** Writing - Review & Editing; **Md Nasir Uddin:** Conceptualization, Methodology, Writing - original draft, Writing - review & editing, Supervision.

## Figure Captions

**Figure 1:** Schematic of the proposed deep learning prior NODDI (DLpN). The stochastic dictionary learning framework i.e., DictNet estimates  $f_{ISO}$  prior and then used with NODDI Rician log-likelihood estimation steps for NDI and  $\kappa$  mapping. A1) DictNet A2) Additional T2 and FA contribution in dictionary building. B) DL prior NODDI.

**Figure 2:** The training and validation loss per epoch for  $f_{ISO}$  with DictNet and extended Microstructure Estimation using a Deep Network (PMEDN): A) single-shell protocol P1, B) multi-shell protocol P12. The results show  $f_{ISO}$  estimation error from DictNet can be minimized lower than PMEDN with single-shell and as lower as multi-shell while utilizing less memory and time. Note: P1 = protocol with  $b=1000$  s/mm<sup>2</sup> and P12= protocol with  $b=1000, 2000$  s/mm<sup>2</sup>.

**Figure 3:** Comparison of DLpN and NODDI for neurite density index (NDI) reconstruction in simulation with defined protocols (P1, P2, P3, P12, P13, P23 and Pall) where NDI ground-truth (GT) values are indicated with dashed lines: A) 0.2, B) 0.4, C) 0.6, and D) 0.8. Synthetic data simulation utilizes the combination of parameters defined in Table 2 to generate diffusion signals with 20dB Rician noise. Single-shell (P1, P2, P3) NDI reconstruction fails in NODDI, but seems plausible with DLpN framework using known  $f_{ISO}$  prior.

**Figure 4:** Comparison of DLpN and NODDI in ODI reconstruction in simulation with defined protocols (P1, P2, P3, P12, P13, P23 and Pall) for ODI ( $\kappa$ ) ground-truth (GT) values are reported: A) 0, B) 0.25, C) 1, D) 4, E) 16. Note  $ODI = \frac{2}{\pi} \arctan\left(\frac{1}{\kappa}\right)$ . Variability of ODI for higher ground truth at A) and B) is related to the ODI itself. The orientation distributions corresponding to very

large ODIs are not very different from one another and the high variance at higher ODI also reflects lack of any difference.

**Figure 5:** DictNet estimation of  $f_{iso}$  at ground-truth values A) 0, B) 0.12, C) 0.4, D) 0.75, E) 1 (indicated with a dashed line) on the simulation test set with defined protocols P1, P2, P3, P12, P13, P23 and Pall for different NDI ground-truth values provided in Figure 3. DictNet generated  $f_{iso}$  priors are mostly in coherence with the ground-truth values for P12.

**Figure 6:** A) A representative axial view of the isotropic volume fraction ( $f_{iso}$ ) maps estimated with proposed DictNet and NODDI for different protocols. Note, NODDI<sub>Pall</sub>  $f_{iso}$  is considered as pseudo ground-truth  $f_{iso}$  and used as training data for DictNet; B) Difference maps for DictNet  $f_{iso}$  and NODDI  $f_{iso}$  with respect to NODDI<sub>Pall</sub>  $f_{iso}$  for defined protocols. Intensity scales are shown.

**Figure 7:** A) A representative axial view of the neurite density index (NDI) maps estimated with proposed DLpN and NODDI for different protocols on an HCP subject. Note, NODDI Pall is considered as pseudo ground-truth for comparison. B) Difference map for DLpN NDI and NODDI NDI with respect to NODDI<sub>Pall</sub> NDI for defined protocols. Intensity scales are shown.

**Figure 8:** A) A representative axial view of the orientation dispersion index (ODI) maps estimated with proposed DLpN and NODDI for different protocols on an HCP subject. Note NODDI<sub>Pall</sub> is considered as pseudo ground-truth for comparison; B) Difference maps for all DLpN and NODDI ODI maps) with respect to NODDI<sub>Pall</sub>. Intensity scales are shown.

**Figure 9:** The estimation errors (%) from *in vivo* data in fiso (A, B), NDI (C, D) and ODI (E, F) for white matter (WM) and grey matter (GM) using DLpN single-shell P1, P2, P3, and multi-shell protocols P12, P12, P23 and Pall. Errors were calculated with respect to the pseudo ground-truth (NODDI<sub>Pall</sub>) for six HCP test subjects.

**Supplementary Figure S1:** The sum of mean square error (MSE) for 4 human subjects (HCP data) to figure out an appropriate number of subjects for training. The plot clearly depicts that for voxel-based training strategies, if the number of subjects is increased there are chances of overfitting. DLpN based NDI, fiso and ODI results indicate increasing trends when training subjects  $> 3$ . The network settings were kept the same for all 5 training times.

**Supplementary Figure S2:** Comparison of isotropic volume fraction (fiso) for DictNet single-shell protocols (P1, P2, P3) and multi-shell NODDI<sub>Pall</sub> for different white matter (WM) and grey matter (GM) ROIs using JHU WM and WM tract atlas and HO GM atlas.

**Supplementary Figure S3:** Comparison of neurite density index (NDI) for DLpN single-shell protocols (P1, P2, P3) and multi-shell NODDI<sub>Pall</sub> for different white matter (WM) and grey matter (GM) ROIs using JHU WM and WM tract atlas and HO GM atlas.

**Supplementary Figure S4:** Comparison of orientation dispersion index (ODI) for DLpN single-shell protocols (P1, P2, P3) and multi-shell NODDI<sub>Pall</sub> for different white matter (WM) and grey matter (GM) ROIs using JHU WM and WM tract atlas and HO GM atlas.

**Supplementary Figure S5:** Scatter plots showing significant linear correlations between DLpN derived NDI, ODI and fISO at different protocols (P1, P2, P3, P12, P13, P23 and Pall) with the pseudo ground-truth NODDI fitting ( $\text{NODDI}_{\text{Pall}}$ ). Asteric symbols are the mean of all the ROIs from John Hopkins University (JHU) White Matter and Harvard Oxford (HO) cortical and subcortical grey matter atlases. Grey indicating GM and blue indicating WM ROIs. Both single-shell and multi-shell protocol for DLpN showed very strong concordance with the pseudo ground-truth  $\text{NODDI}_{\text{Pall}}$ .

**Supplementary Figure S6:** Sagittal, Coronal, Axial images of DLpNP2 and NODDI<sub>Pall</sub> of an HCP subject. White arrows show possible noisy overestimated NDI region, recovered in DLpNP2. Most white regions correspond to undefined NDI.

**Supplementary Figure S7:** Underestimated fiso near GM regions where  $\text{NODDI fiso} = 0$  (shown in blue).  $\text{NODDI}_{\text{Pall}} \text{ fiso}$  shown with FSL colormap - Copper. NODDI nonlinear parametric search seems to have lowered fiso estimation by accounting for higher dispersion in these regions. The blue regions also depict the regions where DictNet estimated slightly higher fiso than NODDI.

## References

Alexander, D.C., Dyrby, T.B., Nilsson, M., Zhang, H., 2019. Imaging brain microstructure with diffusion MRI: practicality and applications. *NMR in Biomedicine* 32, e3841.

Alexander, D.C., Zikic, D., Ghosh, A., Tanno, R., Wottschel, V., Zhang, J., Kaden, E., Dyrby, T.B., Sotiropoulos, S.N., Zhang, H., 2017. Image quality transfer and applications in diffusion MRI. *NeuroImage* 152, 283-298.

Assaf, Y., Pasternak, O., 2008. Diffusion tensor imaging (DTI)-based white matter mapping in brain research: a review. *Journal of molecular neuroscience* 34, 51-61.

Basser, P.J., Mattiello, J., LeBihan, D., 1994. MR diffusion tensor spectroscopy and imaging. *Biophys J* 66, 259-267.

Beaulieu, C., 2002. The basis of anisotropic water diffusion in the nervous system—a technical review. *NMR in Biomedicine: An International Journal Devoted to the Development and Application of Magnetic Resonance In Vivo* 15, 435-455.

Blumensath, T., Davies, M.E., 2008. Iterative Thresholding for Sparse Approximations. *Journal of Fourier Analysis and Applications* 14, 629-654.

Chad, J.A.P., Ofer; Chen, J. Jean, 2019. Free water mapping in diffusion MRI: How do two common approaches compare?, International Society for Magnetic Resonace in Medicine. ISMRM, Montreal, QC, Canada, p. 3656.

Conel, J.L., 1947. The cerebral cortex of the 3-month infant. *Anat Rec* 97, 382.

Daducci, A., Canales-Rodriguez, E.J., Zhang, H., Dyrby, T.B., Alexander, D.C., Thiran, J.P., 2015. Accelerated Microstructure Imaging via Convex Optimization (AMICO) from diffusion MRI data. *Neuroimage* 105, 32-44.

Domke, J., 2012. Generic Methods for Optimization-Based Modeling. In: Neil, D.L., Mark, G. (Eds.), *Proceedings of the Fifteenth International Conference on Artificial Intelligence and Statistics*. PMLR, *Proceedings of Machine Learning Research*, pp. 318--326.

Dutta, R., Trapp, B.D., 2007. Pathogenesis of axonal and neuronal damage in multiple sclerosis. *Neurology* 68, S22-S31.

Edwards, L.J., Pine, K.J., Ellerbrock, I., Weiskopf, N., Mohammadi, S., 2017. NODDI-DTI: estimating neurite orientation and dispersion parameters from a diffusion tensor in healthy white matter. *Frontiers in neuroscience* 11, 720.

Farrher, E., Grinberg, F., Kuo, L.W., Cho, K.H., Buschbeck, R.P., Chen, M.J., Chiang, H.H., Choi, C.H., Shah, N.J., 2020. Dedicated diffusion phantoms for the investigation of free water elimination and mapping: insights into the influence of T2 relaxation properties. *NMR in Biomedicine* 33, e4210.

Fiala, J.C., Spacek, J., Harris, K.M., 2002. Dendritic spine pathology: cause or consequence of neurological disorders? *Brain Res Brain Res Rev* 39, 29-54.

Glasser, M.F., Sotiroopoulos, S.N., Wilson, J.A., Coalson, T.S., Fischl, B., Andersson, J.L., Xu, J., Jbabdi, S., Webster, M., Polimeni, J.R., 2013. The minimal preprocessing pipelines for the Human Connectome Project. *Neuroimage* 80, 105-124.

Golkov, V., Dosovitskiy, A., Sperl, J.I., Menzel, M.I., Czisch, M., Samann, P., Brox, T., Cremers, D., 2016. q-Space Deep Learning: Twelve-Fold Shorter and Model-Free Diffusion MRI Scans. *IEEE Trans Med Imaging* 35, 1344-1351.

Grussu, F., Schneider, T., Zhang, H., Alexander, D.C., Wheeler-Kingshott, C.A., 2015. Neurite orientation dispersion and density imaging of the healthy cervical spinal cord in vivo. *Neuroimage* 111, 590-601.

Jacobs, B., Driscoll, L., Schall, M., 1997. Life-span dendritic and spine changes in areas 10 and 18 of human cortex: A quantitative golgi study. *Journal of Comparative Neurology* 386, 661-680.

Jespersen, S.N., Bjarkam, C.R., Nyengaard, J.R., Chakravarty, M.M., Hansen, B., Vosegaard, T., Ostergaard, L., Yablonskiy, D., Nielsen, N.C., Vestergaard-Poulsen, P., 2010. Neurite density from magnetic resonance diffusion measurements at ultrahigh field: comparison with light microscopy and electron microscopy. *Neuroimage* 49, 205-216.

Jespersen, S.N., Leigland, L.A., Cornea, A., Kroenke, C.D., 2012. Determination of axonal and dendritic orientation distributions within the developing cerebral cortex by diffusion tensor imaging. *IEEE Trans Med Imaging* 31, 16-32.

Novikov, D.S., Veraart, J., Jelescu, I.O., Fieremans, E., 2018. Rotationally-invariant mapping of scalar and orientational metrics of neuronal microstructure with diffusion MRI. *NeuroImage* 174, 518-538.

Parker, D., Ould Ismail, A.A., Wolf, R., Brem, S., Alexander, S., Hodges, W., Pasternak, O., Caruyer, E., Verma, R., 2020. Freewater estimatoR using iNtErpolated iniTialization (FERNET): Characterizing peritumoral edema using clinically feasible diffusion MRI data. *PloS one* 15, e0233645.

Pasternak, O., Kelly, S., Sydnor, V.J., Shenton, M.E., 2018. Advances in microstructural diffusion neuroimaging for psychiatric disorders. *Neuroimage* 182, 259-282.

Timmers, I., Roebroeck, A., Bastiani, M., Jansma, B., Rubio-Gozalbo, E., Zhang, H., 2016. Assessing microstructural substrates of white matter abnormalities: a comparative study using DTI and NODDI. *PloS one* 11, e0167884.

Van Essen, D.C., Smith, S.M., Barch, D.M., Behrens, T.E.J., Yacoub, E., Ugurbil, K., 2013. The WU-Minn Human Connectome Project: An overview. *Neuroimage* 80, 62-79.

Veraart, J., Fieremans, E., Novikov, D.S., 2019. On the scaling behavior of water diffusion in human brain white matter. *Neuroimage* 185, 379-387.

Ye, C., 2017. Estimation of tissue microstructure using a deep network inspired by a sparse reconstruction framework. International Conference on Information Processing in Medical Imaging. Springer, pp. 466-477.

Ye, C., Li, X., Chen, J., 2019. A deep network for tissue microstructure estimation using modified LSTM units. *Medical image analysis* 55, 49-64.

Zhang, H., Hubbard, P.L., Parker, G.J., Alexander, D.C., 2011. Axon diameter mapping in the presence of orientation dispersion with diffusion MRI. *Neuroimage* 56, 1301-1315.

Zhang, H., Schneider, T., Wheeler-Kingshott, C.A., Alexander, D.C., 2012. NODDI: practical in vivo neurite orientation dispersion and density imaging of the human brain. *Neuroimage* 61, 1000-1016.

## Tables

**Table 1: The list of imaging protocols used to perform the synthetic data simulation and used for *in vivo* data.**

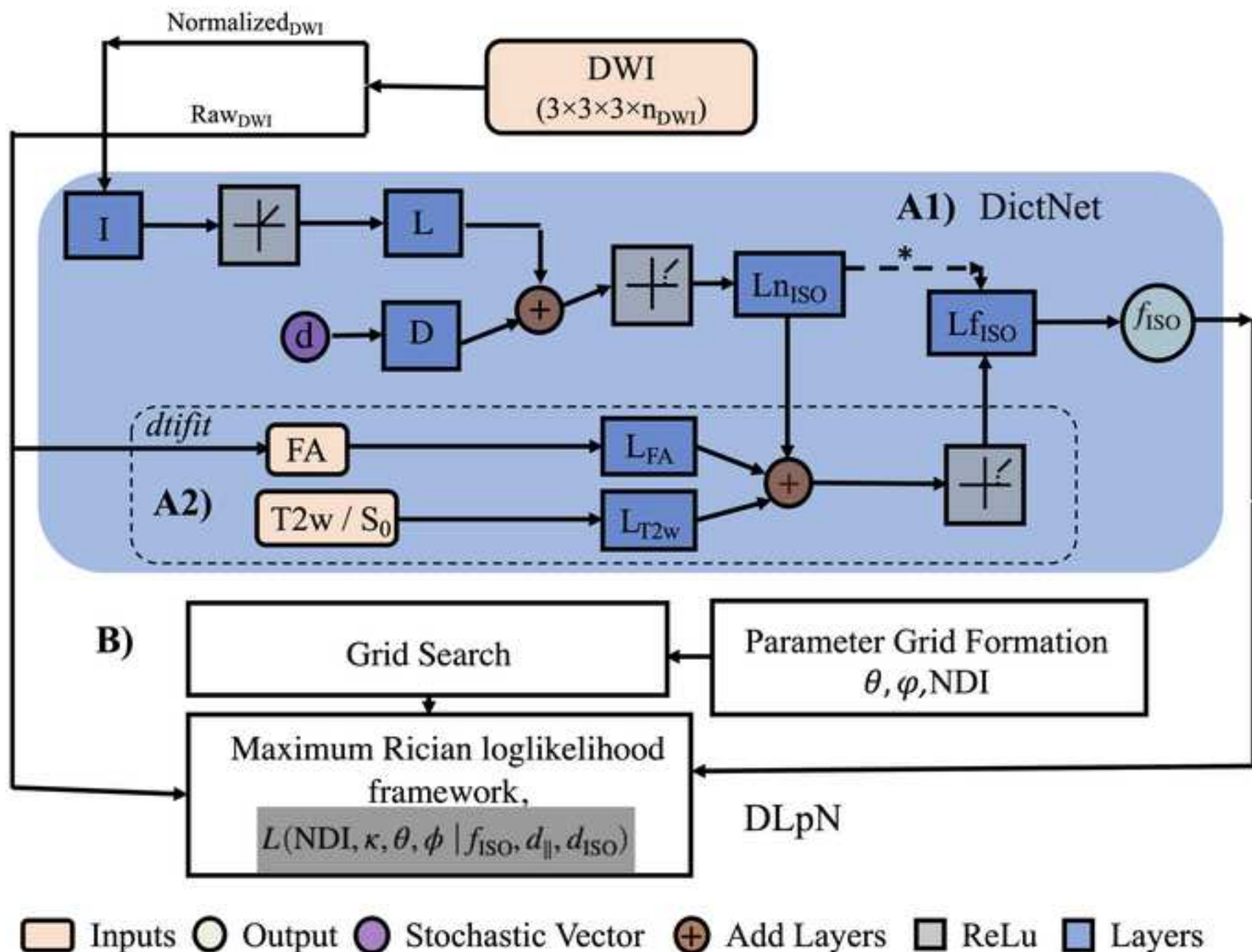
Protocols	b-value (number of gradients)
P1	b1000 (90)
P2	b2000 (90)
P3	b3000 (90)
P12	b1000 (90) + b2000 (90)
P13	b1000 (90) + b3000 (90)
P23	b2000 (90) + b3000 (90)
Pall	b1000 (90) + b2000 (90) + b3000 (90)

Note: b-values are in  $\text{s/mm}^2$ ; P1, P2, P3 are single-shell; P12, P13, P23 are two-shell; Pall is three-shell protocols. The number in parentheses indicate the number of gradient directions (excluding  $b=0$  images).

**Table 2: The ground-truth parameter values for the synthetic data simulation**

Parameters	Ground-truth values
NDI	0.2, 0.4, 0.6, 0.8
$f_{ISO}$	0,0.12,0.4,0.75,1
$a$ (radii) $\mu\text{m}$	0.5, 1, 2, 4
$\kappa$	0, 0.25, 1, 4, 16
$\mu$ ( $\Theta, \phi$ )	254 uniformly distributed orientations

Note: NDI, Neurite Density Index;  $f_{ISO}$ , Isotropic Volume Fraction;  $a$ , axon radii;  $\kappa$ , concentration parameter;  $\mu$ , orientation.



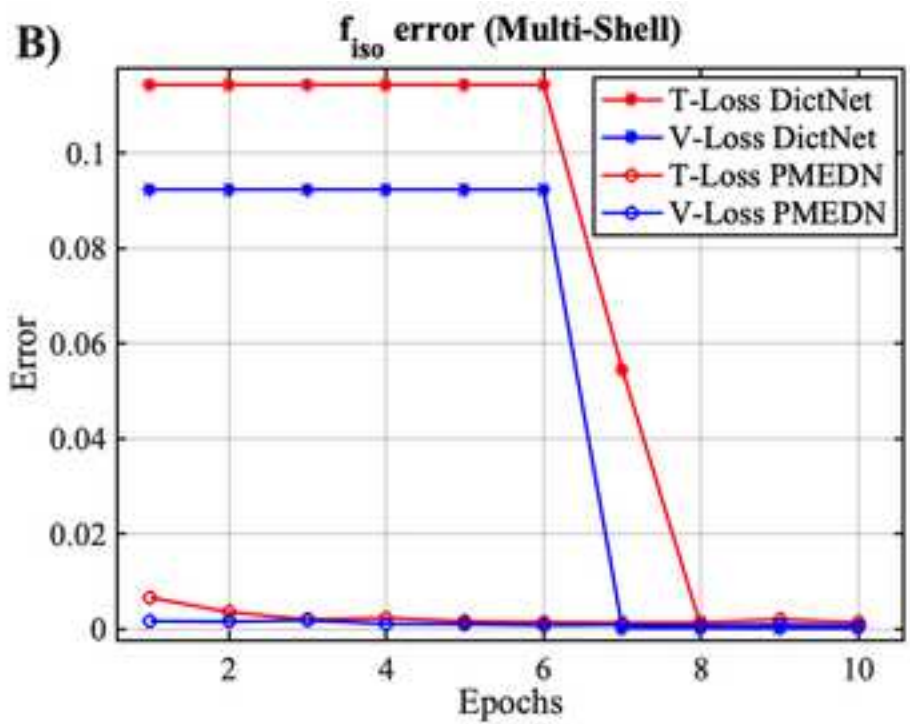
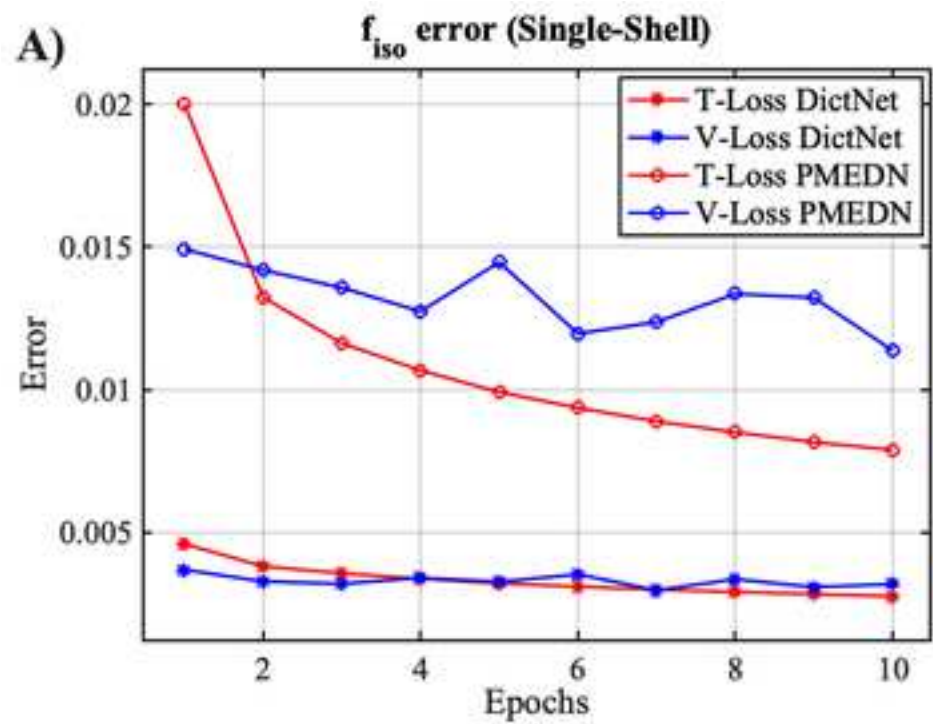
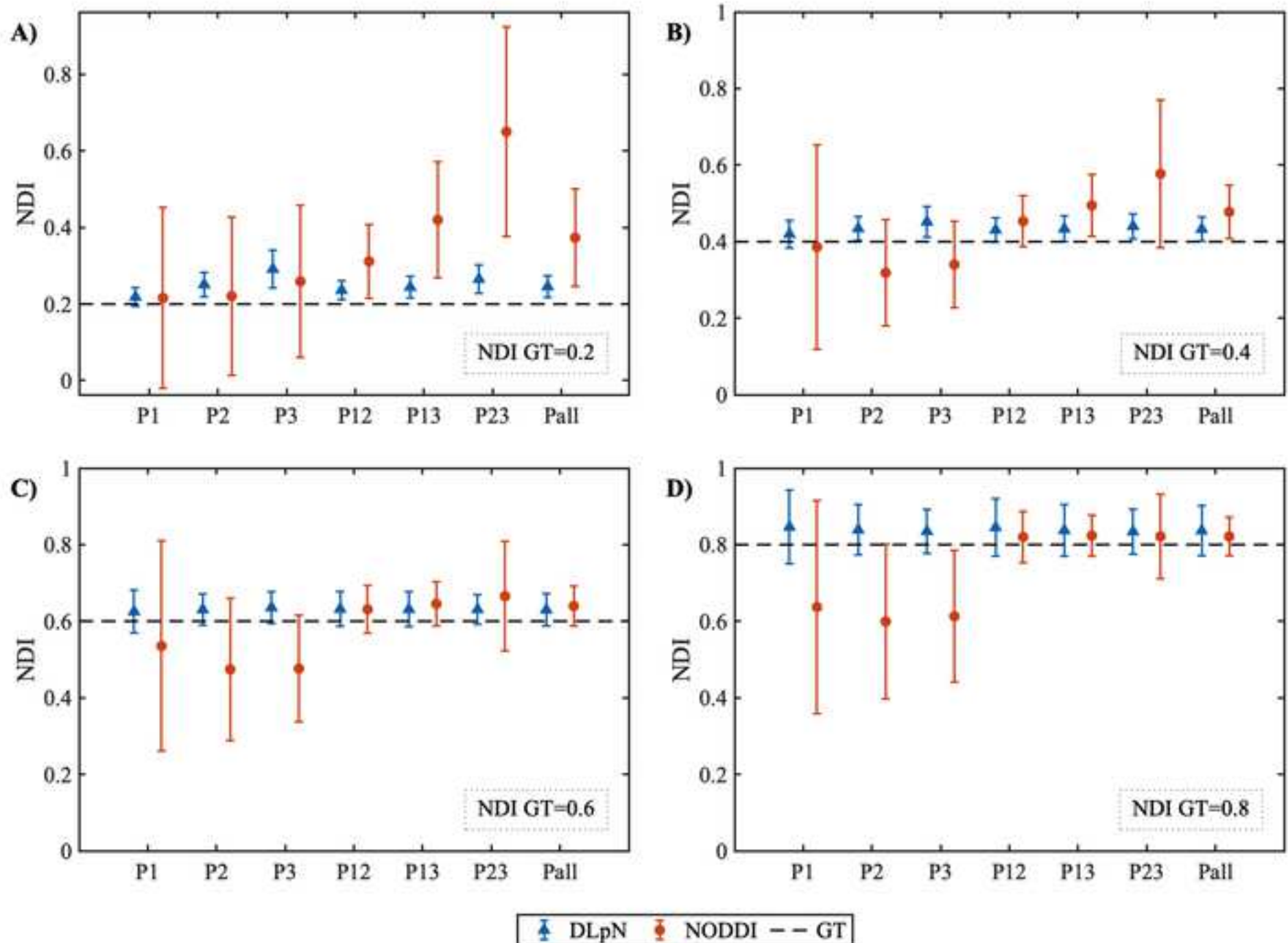


Figure 3

Click here to access/download;9. Figure;Figure3.tif 

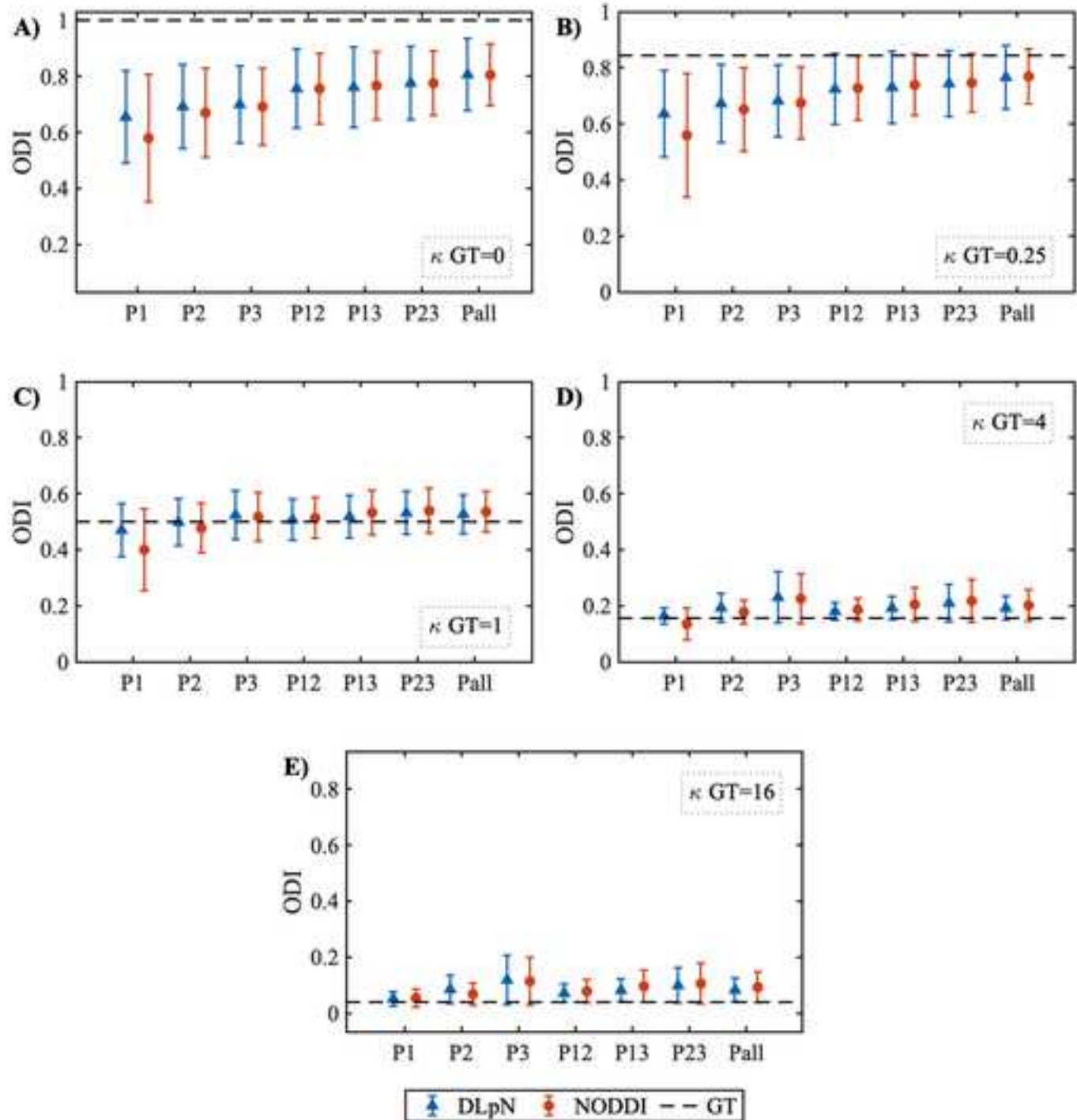


Figure 5

Click here to access/download;9. Figure;Figure5.tif

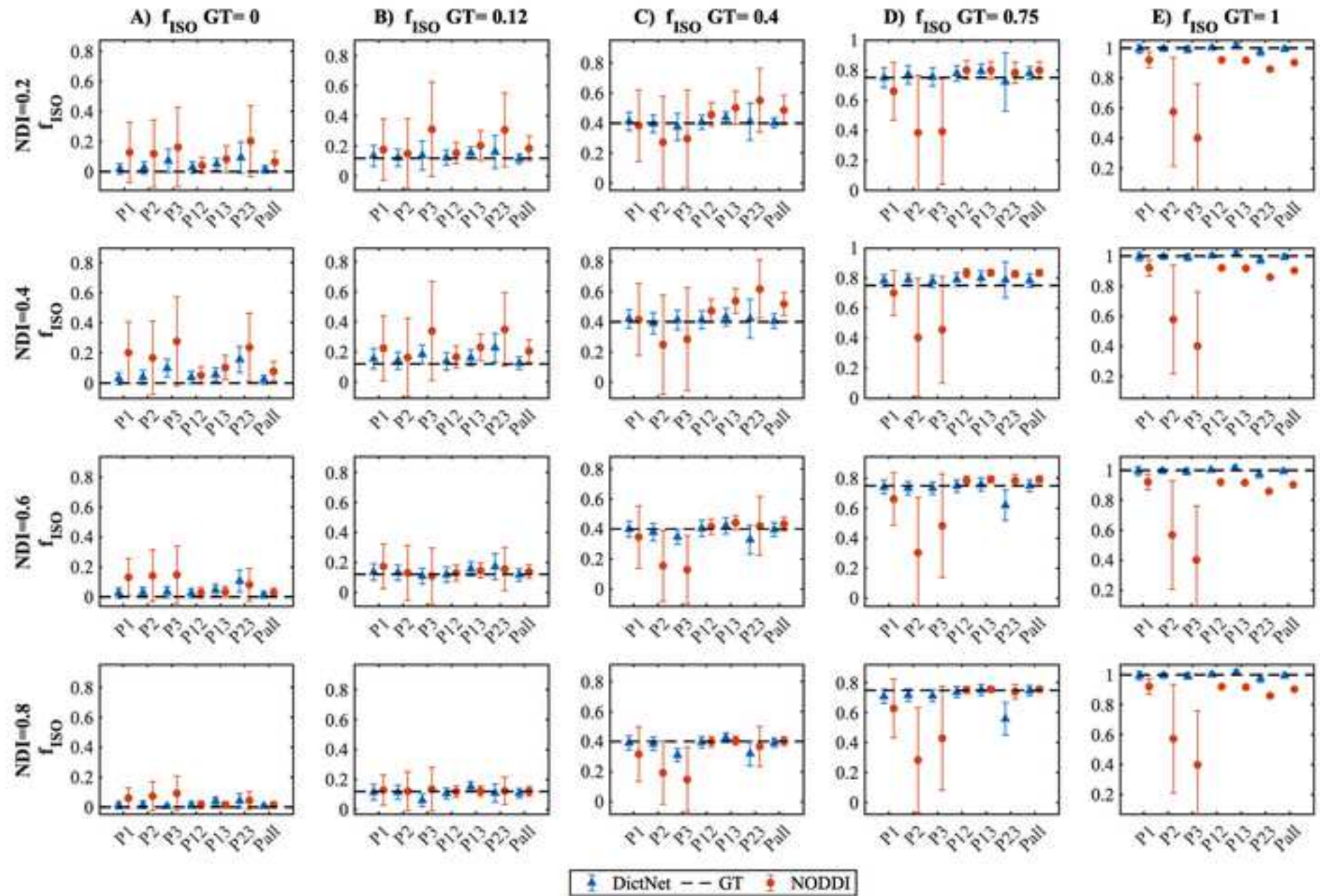


Figure 6

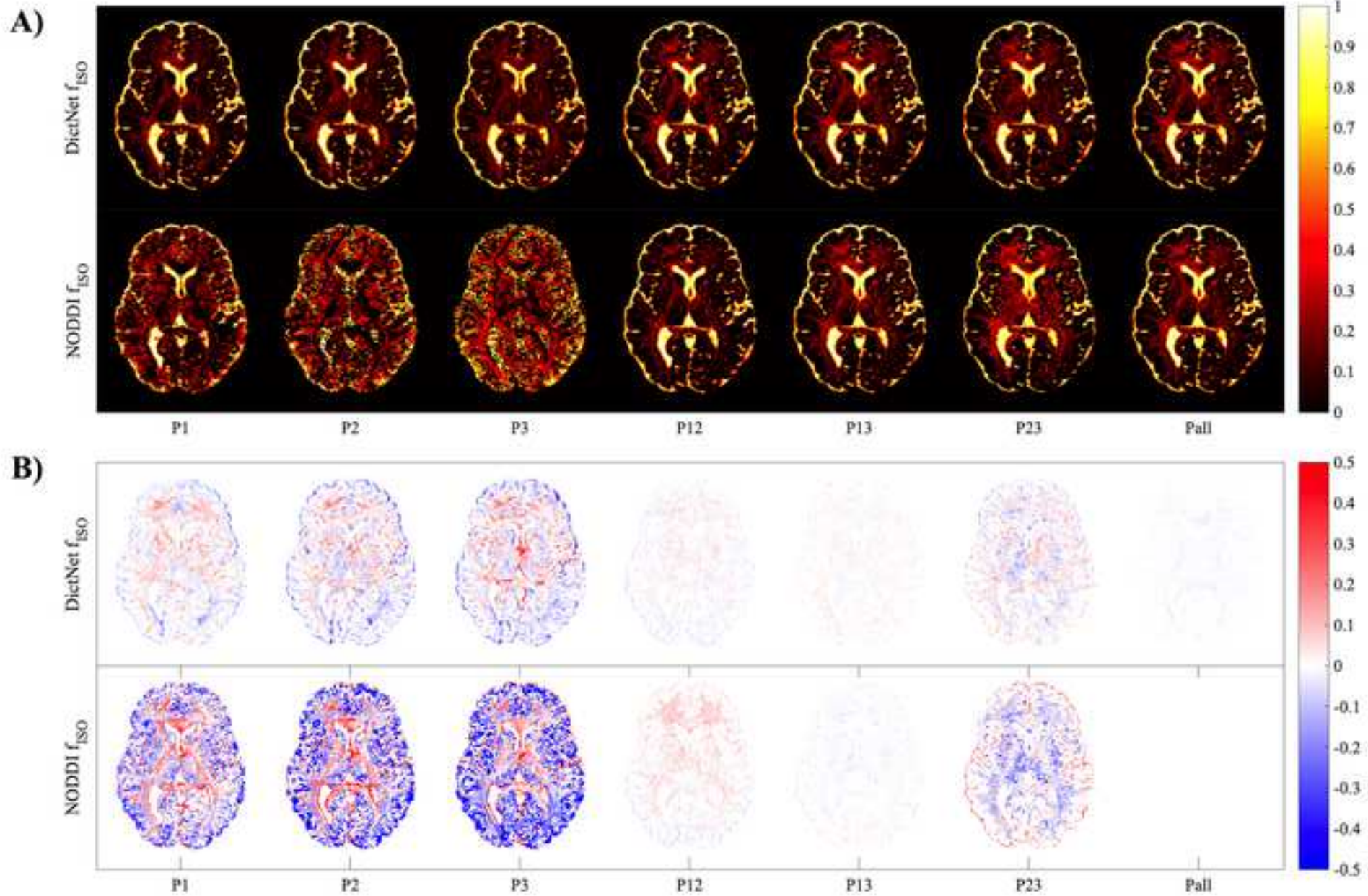
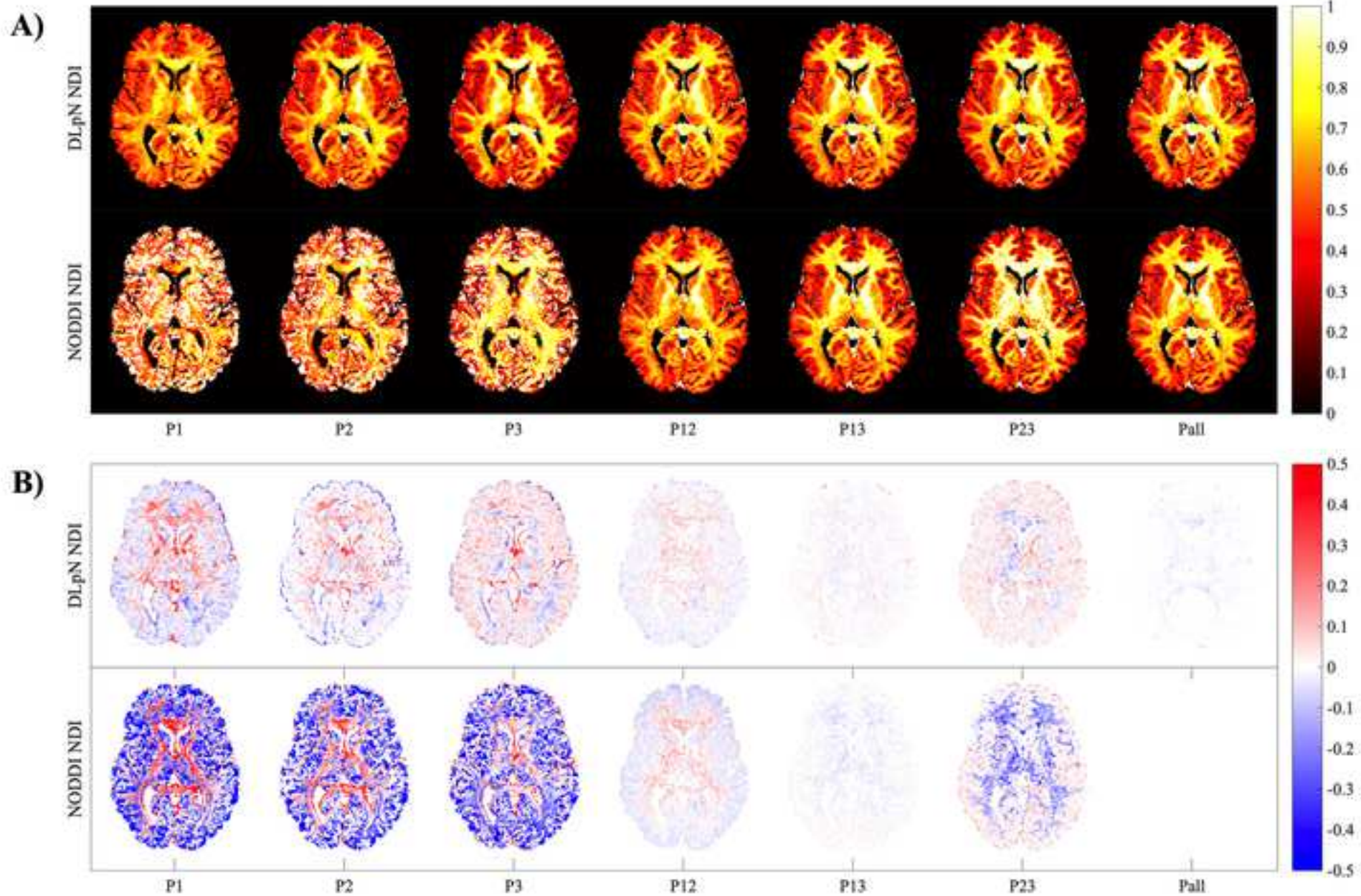
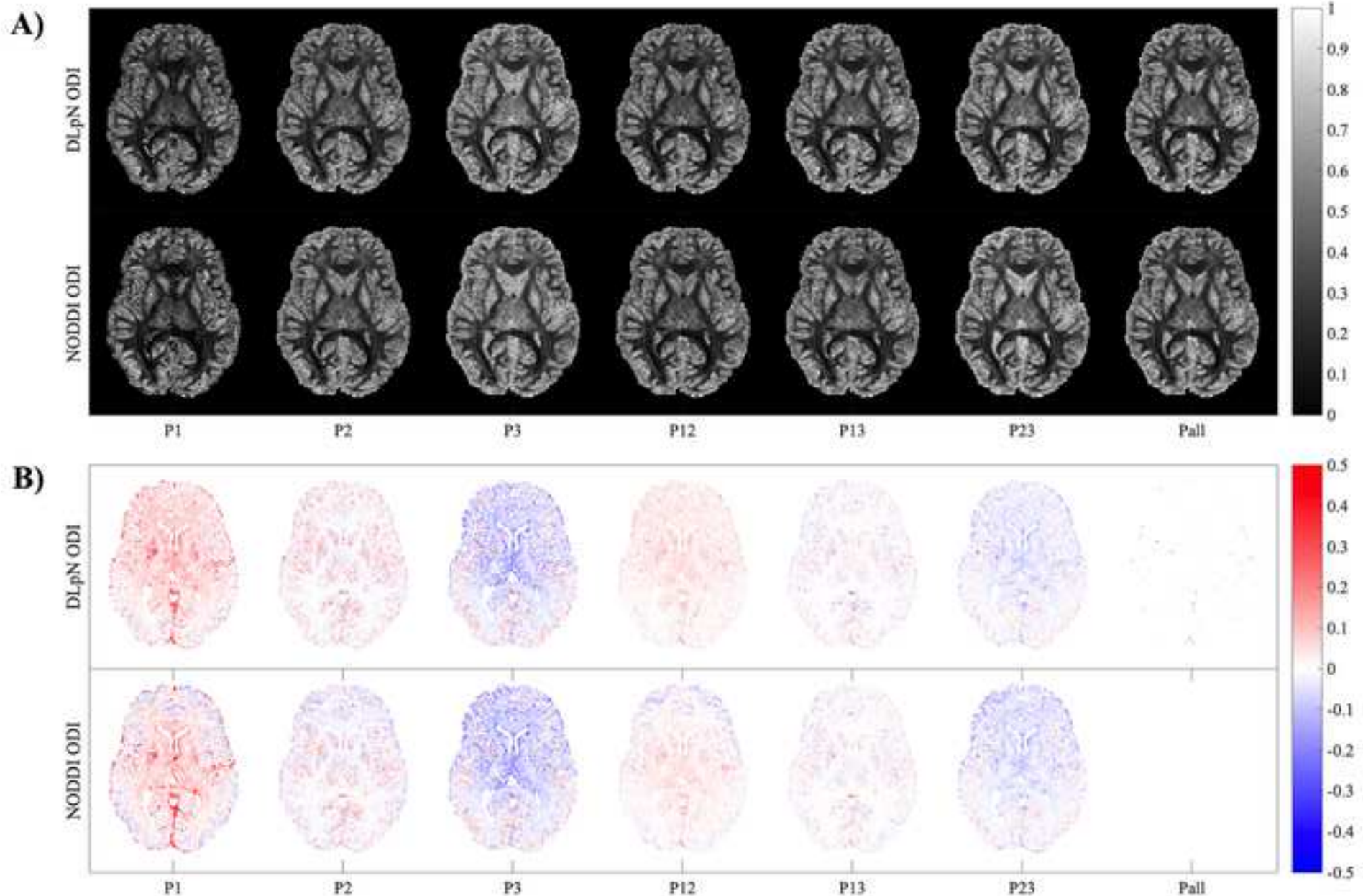
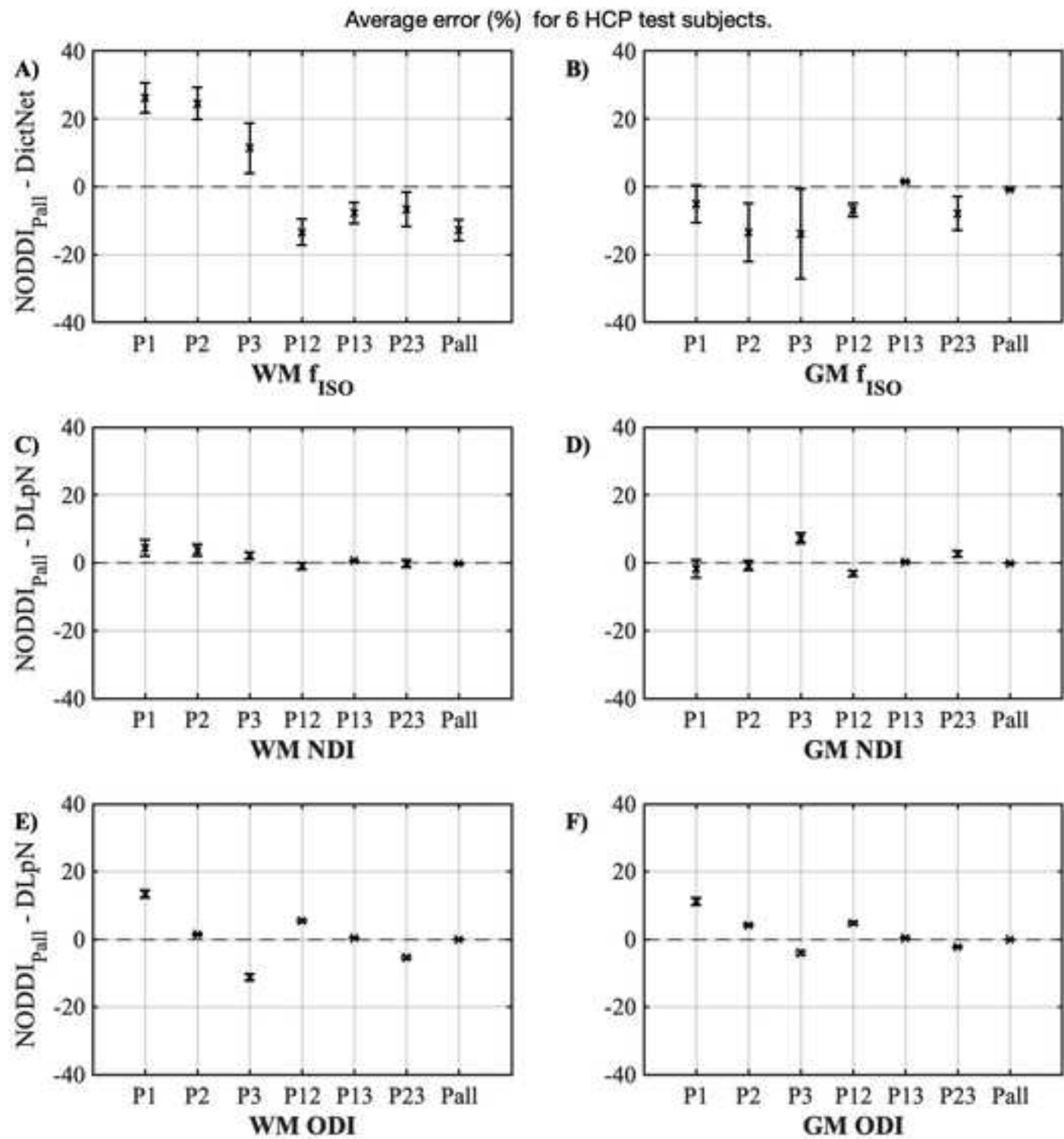
[Click here to access/download;9. Figure;Figure6.tif](#) 

Figure 7

[Click here to access/download;9. Figure;Figure7.tiff](#)

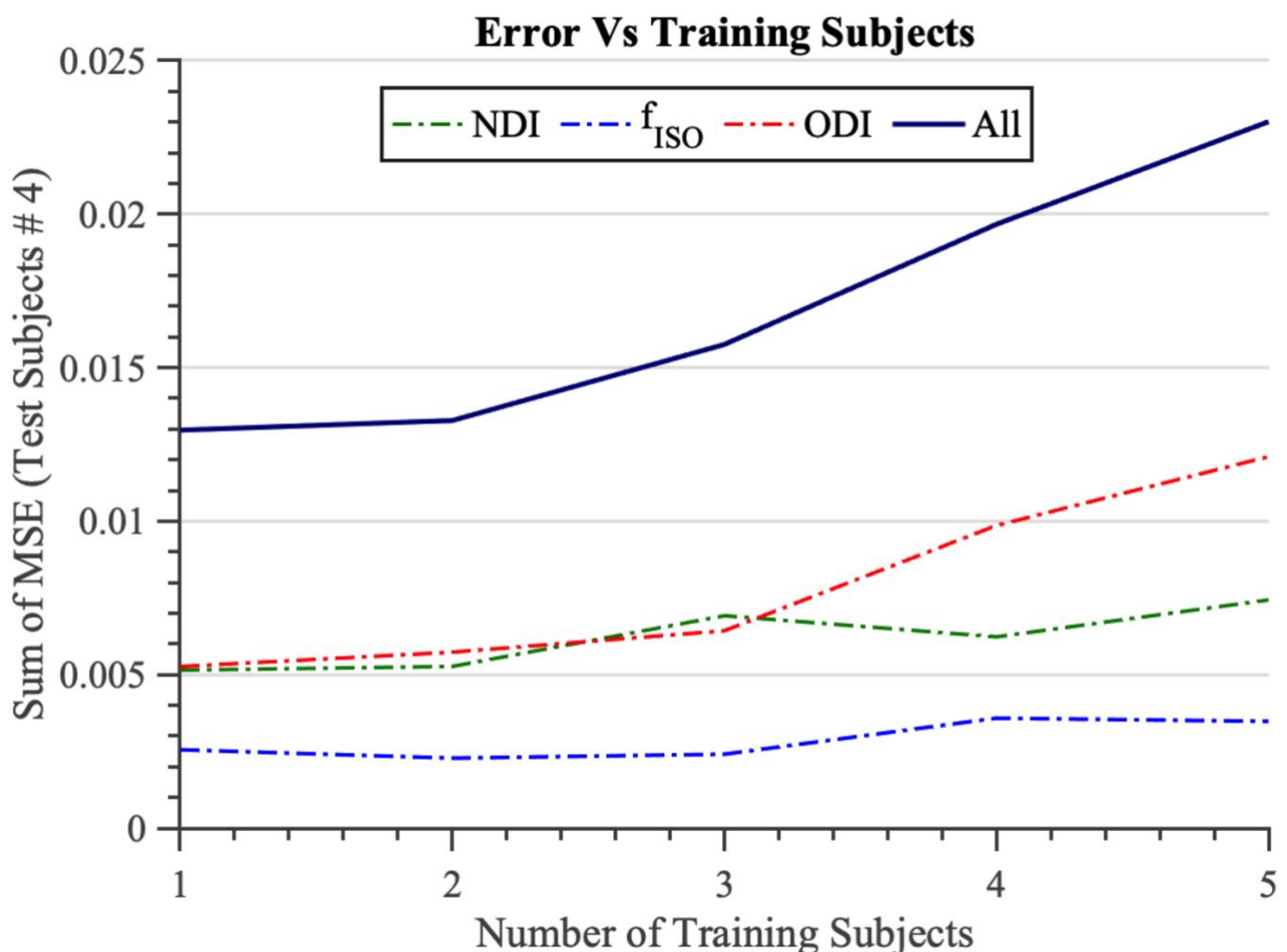




## Supplementary Material

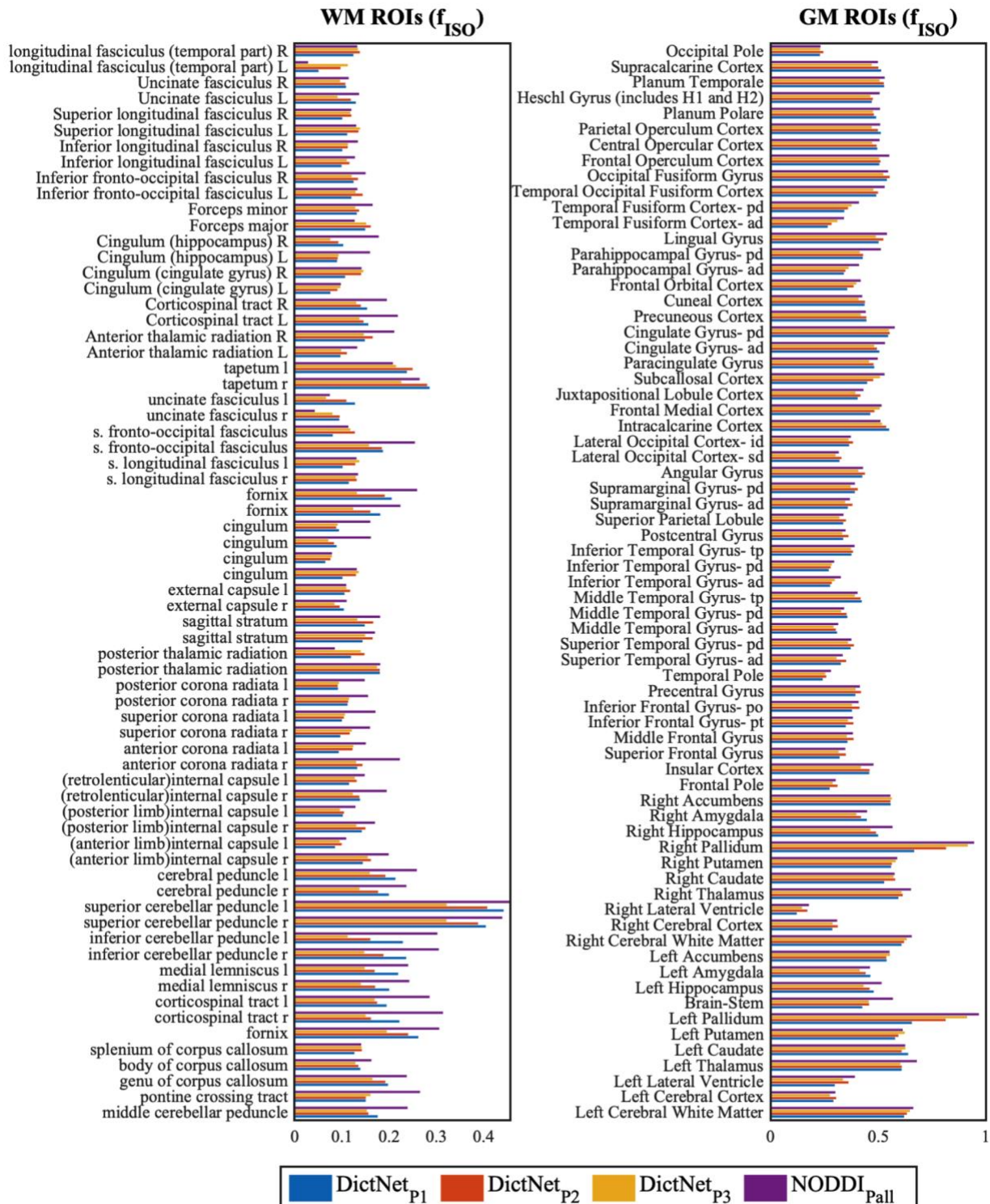
### Supplementary Figure S1. Determining number of training subjects for DictNet

The sum of mean square error (MSE) for 4 human test subjects (HCP data) for variable training subjects shown to figure out an appropriate number of subjects required for training. The plot clearly depicts that for voxel-based training strategies, if the number of subjects is increased there are chances of overfitting. DLpN based NDI, f<sub>ISO</sub> and ODI results indicate increasing trends when training subjects > 3. The network settings were kept the same for all 5 training times.



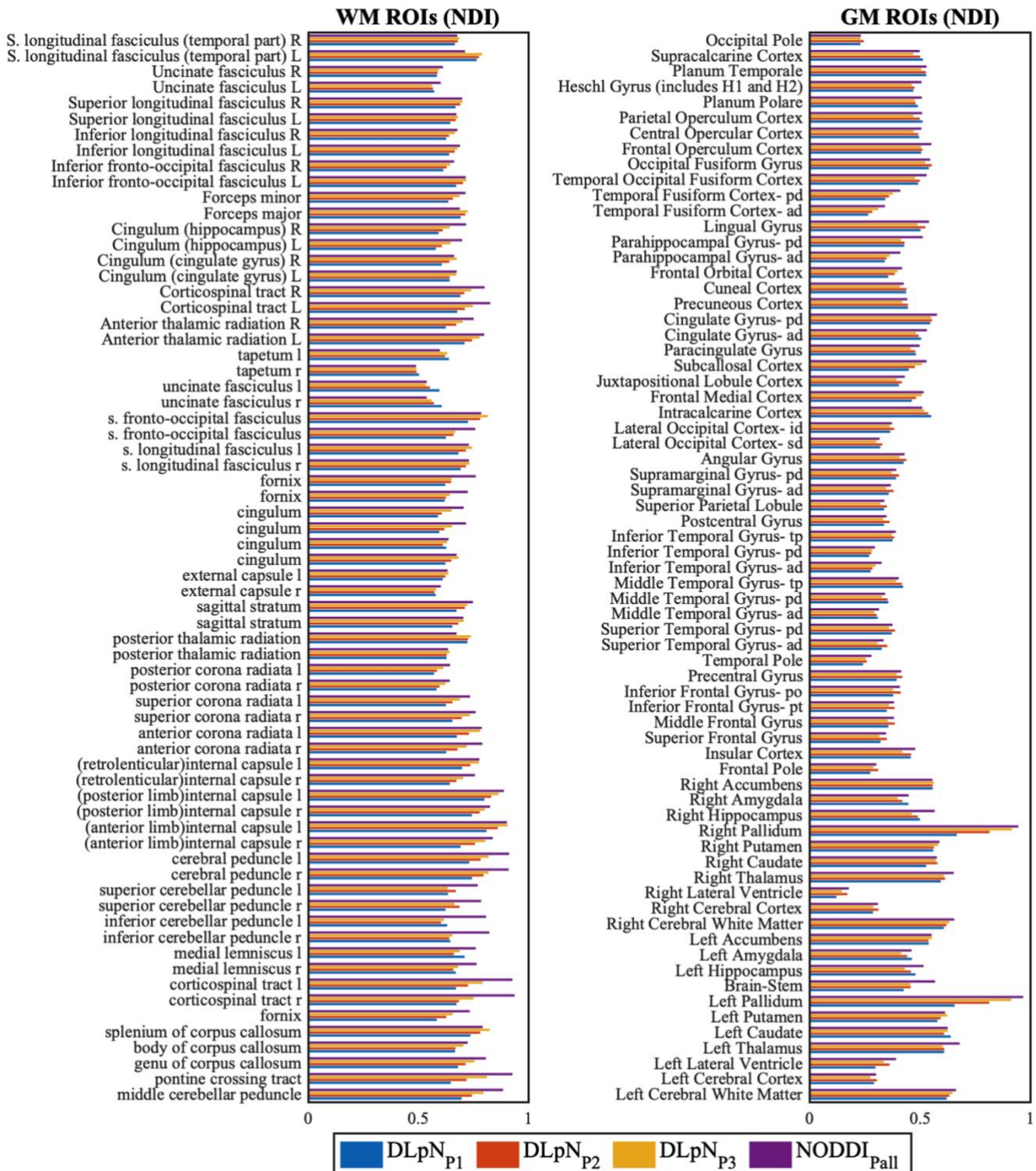
## Supplementary Figure S2. Comparison of f<sub>ISO</sub> values in brain ROIs

Comparison of DictNet derived isotropic volume fraction (f<sub>ISO</sub>) with single-shell protocols (P1, P2, P3) and NODDI derived f<sub>ISO</sub> with multi-shell (NODDI<sub>Pall</sub>) for different white matter (WM) and grey matter (GM) ROIs using John Hopkins University (JHU) WM and WM tract atlas and Harvard-Oxford (HO) GM atlas.



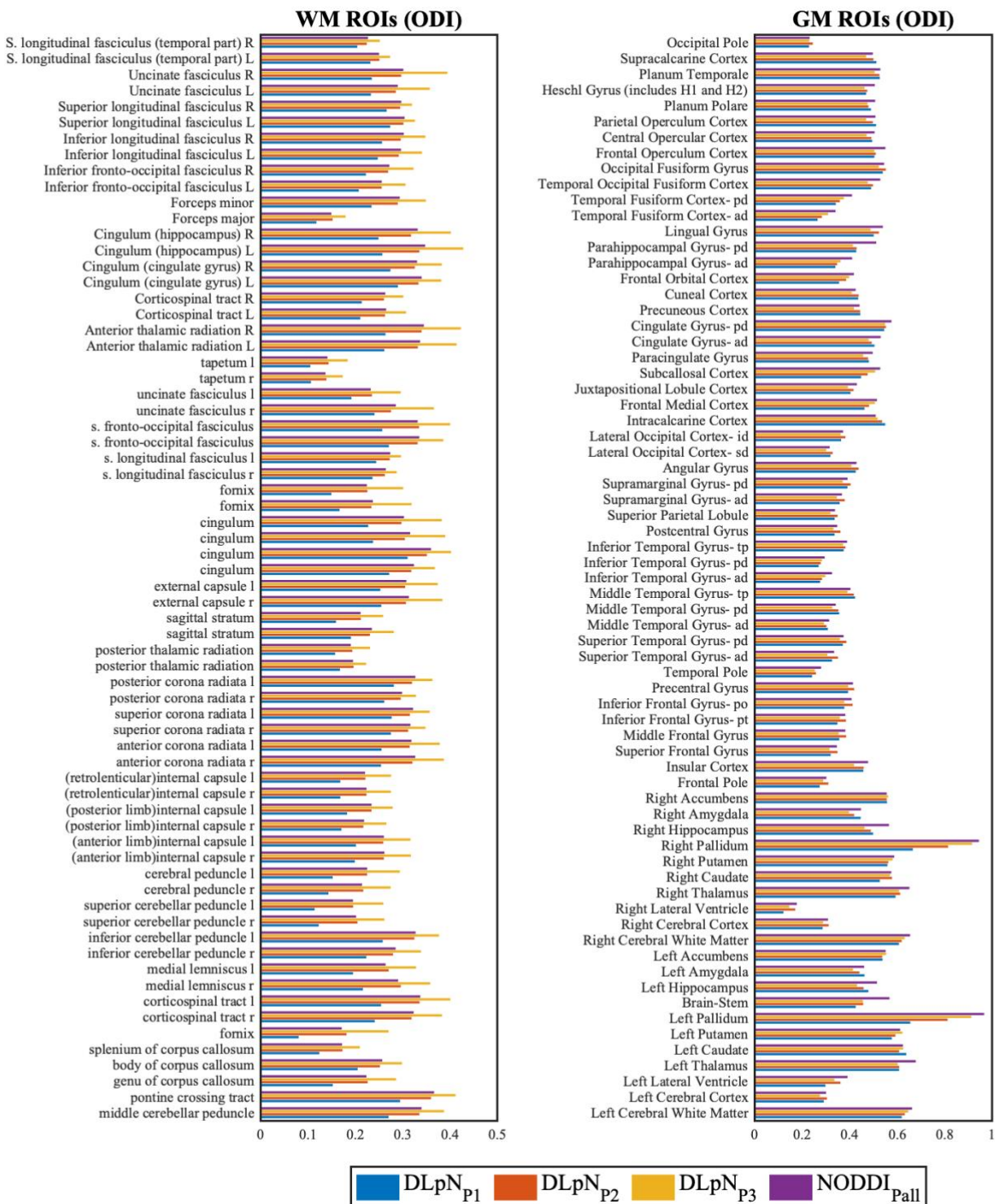
### Supplementary Figure S3. Comparison of NDI values in brain ROIs

Comparison of neurite density index (NDI) for DLpN single-shell protocols (P1, P2, P3) and multi-shell NODDI<sub>Pall</sub> for different white matter (WM) and grey matter (GM) ROIs using John Hopkins University (JHU) WM and WM tract atlas and Harvard-Oxford (HO) GM atlas.



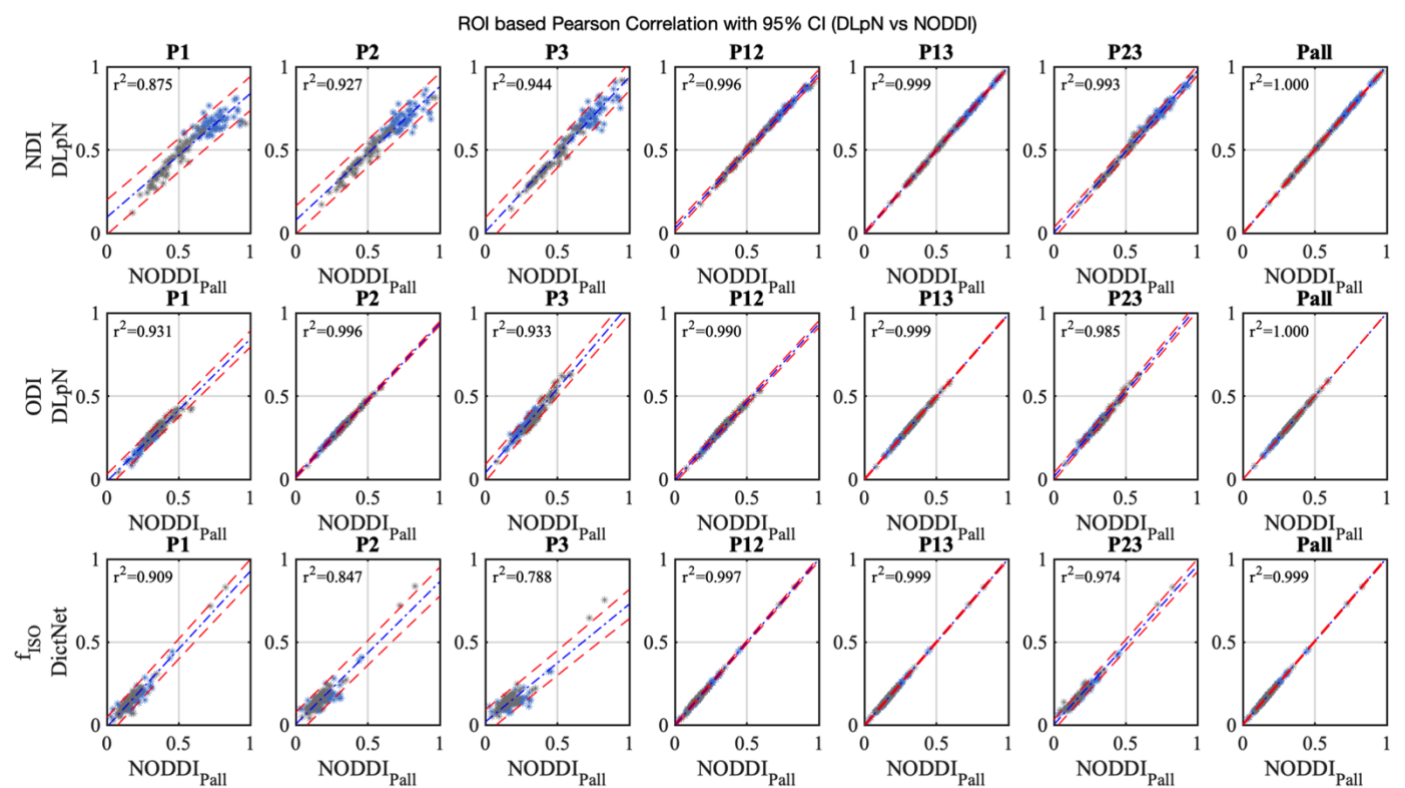
## Supplementary Figure S4. Comparison of ODI values in brain ROIs

Comparison of orientation dispersion index (ODI) for DLpN single-shell protocols (P1, P2, P3) and multi-shell NODDI<sub>Pall</sub> for different white matter (WM) and grey matter (GM) ROIs using John Hopkins University (JHU) WM and WM tract atlas and Harvard-Oxford (HO) GM atlas.



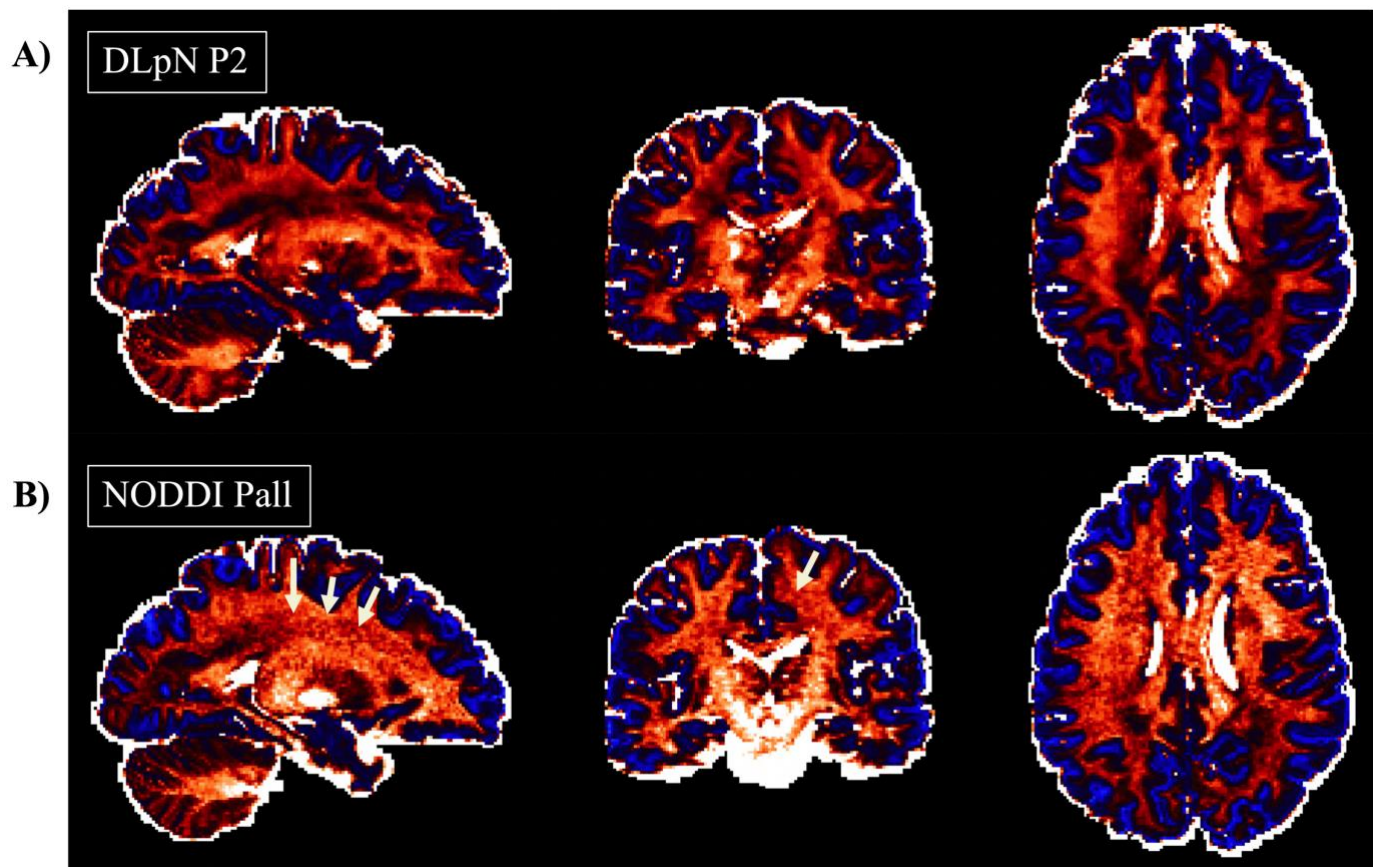
## Supplementary Figure S5. Correlation between DLpN derived NDI, ODI and DictNet derived fiso with respective NODDI<sub>Pall</sub> derived maps

Scatter plots showing significant linear correlations between DLpN derived NDI, ODI, and DictNet derived fiso at different protocols (P1, P2, P3, P12, P13, P23 and Pall) with the pseudo ground-truth NODDI fitting with Pall (NODDI<sub>Pall</sub>). Asteric symbols are the mean of all the ROIs from John Hopkins University White Matter (WM) and Harvard Oxford cortical and sub-cortical grey matter (GM) atlases. Gray indicating GM and blue indicating WM ROIs. Both single-shell and multi-shell protocol for DLpN showed very strong concordance with the pseudo ground-truth NODDI<sub>Pall</sub>.



### Supplementary Figure S6. Comparison of NDI maps from DLpNP<sub>2</sub> and NODDI<sub>Pall</sub>

Sagittal, Coronal, Axial images of DLpNP<sub>2</sub> and NODDI<sub>Pall</sub> of an HCP subject. White arrows show possible noisy overestimated NDI region, recovered in DLpNP<sub>2</sub>. Most white regions correspond to undefined NDI.



### Supplementary Figure S7. Highlighted $f_{ISO}$ map from NODDI<sub>Pall</sub>

Underestimated  $f_{ISO}$  near GM regions where NODDI  $f_{ISO} = 0$  (shown in blue). NODDI<sub>Pall</sub>  $f_{ISO}$  shown with FSL colormap - Copper. NODDI nonlinear parametric search seems to have lowered  $f_{ISO}$  estimation by accounting for higher dispersion in these regions. The blue regions also depict the regions where DictNet estimated slightly higher  $f_{ISO}$  than NODDI.

